# Modern Neuroimaging of Pediatric Brain Tumors

# 13

Mark D. Mamlouk, Sean O. Bryant, Soonmee Cha, and A. James Barkovich

## Contents

M.D. Mamlouk, MD
Division of Neuroradiology,
Kaiser Permanente Santa Clara,
700 Lawrence Expressway, Suite 104, Santa Clara,
CA 95051, USA
e-mail: mark.mamlouk@ucsf.edu

S.O. Bryant, MD
Department of Radiology, Diversified Radiology
of Colorado, PC, 1746 Cole Boulevard, Suite 150,
Lakewood, CO 80401, USA
e-mail: sbryant@divrad.com

S. Cha, MD
Radiology & Neurological Surgery, University
of California San Francisco,
350 Parnassus Avenue, Suite 307, Box 0336,
San Francisco, CA 94143, USA
e-mail: soonmee.cha@ucsf.edu

A.J. Barkovich, MD (✉)
Departments of Radiology and Biomedical Imaging,
Neurology, Pediatrics & Neurosurgery, University of
California San Francisco & UCSF Benioff Children's
Hospital, 505 Parnassus Avenue, Room L352,
San Francisco, CA 94143-0628, USA
e-mail: james.barkovich@ucsf.edu

## 13.1 Modern Neuroimaging of Pediatric CNS Tumors

Neuroimaging has been an important tool in the diagnosis and surveillance of brain tumors for more than 30 years. Although structural magnetic

resonance (MR) imaging remains the most important imaging tool for assessing CNS neoplasms, new techniques have allowed physiologic features of brain tumors and the surrounding functional brain tissue to be performed noninvasively. In this chapter, these new techniques and their applications are discussed.

## 13.2 MR Spectroscopy

### 13.2.1 Principles

Proton MR spectroscopy (MRS) is a powerful and noninvasive imaging technique that can be added to a standard MR study with only a small-time increase (Hunter and Wang 2001). MRS provides information about the activity of specific metabolites that can supplement the information obtained from routine anatomic sequences (Kim et al. 1997; Kimura et al. 2001). MRS may be useful to differentiate tumor from normal tissue, help stratify neoplasms as high- or low-grade, plan biopsies, distinguish between treatment injury and recurrent neoplasm, and separate cystic infection from cystic neoplasm (Yousem et al. 1992; Ott et al. 1993; Lazareff et al. 1999; Nelson et al. 1997a, 1999; Norfray et al. 1999; Poptani et al. 1995; Shimizu et al. 1996; Wang et al. 1996a). Routine MR imaging may lead to incorrect tumor classification in up to 40 % of cases (Ott et al. 1993).

MRS displays peaks from functional groups of numerous neurochemicals (Salibi and Brown 1998). Several of these neurochemicals are important in the analysis of patients with brain tumors, including *N*-acetylaspartate (NAA), trimethylamines (choline [Cho] and related compounds), creatine constituents (Cr), lactate (Lac), myoinositol (Myo), and amino acids (AA) (Hunter and Wang 2001; Norfray et al. 1999; Poptani et al. 1995; Birken and Oldendorf 1989; Dezortova et al. 1999; Tomoi et al. 1997; Urenjak et al. 1993).

A normal NAA peak is thought to reflect a normal number of mature, normally functioning neurons (Hunter and Wang 2001; Birken and Oldendorf 1989). NAA is synthesized in the mitochondria and is believed to be a key compo-

nent in an acetyl group carrier between neuronal mitochondria and cytoplasm. It is vital in the regulation of neuronal protein synthesis and the metabolism of several neurotransmitters (Birken and Oldendorf 1989). NAA is also present in oligodendrocyte precursors (where it is metabolized to acetate (subsequently converted to acetyl CoA) and aspartate by aspartoacylase) and may be elevated or reduced in processes involving oligodendrocytes and myelin, as well as those involving neurons and axons (Urenjak et al. 1993; Tzika et al. 1997). The NAA concentration is dependent on location (it is 10 % lower in the normal cerebellum compared to cerebrum), maturity (increases as the brain develops and neurons mature), and neuronal health (decreased after injury or infiltration by neoplasm) (Wang et al. 1996a; Usenius et al. 1995).

The Cho resonance mainly comprises molecules from cell membranes, such as choline, phosphocholine, and glycerophosphorylcholine (Waldrop et al. 1998). Protons in choline molecules within intact membranes (such as those found in phosphatidylcholine), however, are immobile and do not contribute to MR signal (Norfray et al. 1999; Waldrop et al. 1998; Dowling et al. 2001). Since the Cho peak in the MR spectrum is composed of signal from these compounds during the processes of membrane synthesis and degradation (Norfray et al. 1999; Waldrop et al. 1998; Dowling et al. 2001), elevated Cho is found in neoplasms, active infection, and regions containing inflammatory cells.

The Cr peak comes from methylamine peaks of creatine and phosphocreatine – compounds that provide a high-energy phosphate buffer for adenosine triphosphate synthesis (Norfray et al. 1999). In most disorders, it is not clear what processes produce changes in Cr concentrations. Cr can be depressed in high-grade or metabolically active neoplasm, due to the overwhelming requirements of the proliferating tumor cells (Tzika et al. 1996). It can also be depleted in regions of necrosis secondary to lack of metabolic needs and cell death (Yousem et al. 1992; Tzika et al. 1997, 2001; Taylor et al. 1996).

Lactate is an end product of anaerobic glycolysis that accumulates when the glycolytic rate

exceeds lactate catabolism or overwhelms export by the blood stream (Norfray et al. 1999; Tomoi et al. 1997; Wang et al. 1995). It is a nonspecific marker seen in a variety of conditions such as tumors, necrosis, ischemia, cysts, and treatment injury (Wang et al. 1995). Increasing evidence suggests that the glycolytic pathway is an important source of energy in astrocytes (Belanger et al. 2011), which may explain why astrocytomas often are associated with increased lactate on proton MRS.

Accumulation of 2-hydroxyglutarate (2HG) has been associated with mutations in isocitrate dehydrogenases 1 and 2 (IDH1 and IDH2) in grade II and grade III gliomas. Noninvasive detection of this oncometabolite, 2HG, is now feasible using MRS, and the presence of 2HG peak on MRS has been correlated with mutations in IDH1 or IDH2 in resected tumor tissues of gliomas (Choi et al. 2012). As the MRS techniques continue to improve, detection and quantification of 2HG may become an important part of preoperative diagnosis and assessment of prognosis in patients with glioma.

## 13.2.2 Technique

Currently, at the University of California, San Francisco (UCSF), we obtain spectra from a large area of the brain ($8 \times 8 \times 8$ cm) and can resolve spectra from volumes of less than 1 cm³ within that area. These data are acquired in approximately 8 min on a 3 T MRI (Nelson et al. 1999; McKnight et al. 2001; Nelson et al. 1997b). Using this technique, a small tumor focus can be identified in a large region of heterogeneous tissue. Moreover, postprocessing allows the voxel to be placed in precisely the same region of interest as in prior studies, allowing increased confidence that the tumor has been sampled in precisely the same location (Nelson et al. 1994). On MR scanners without 3D spectroscopic imaging (3D MRSI), 2D MRSI, commercially available from all major manufacturers, can be extremely useful. Two-dimensional MRSI allows coverage of a large area of tissue with small voxel size and an excellent signal-to-noise ratio (Dowling et al. 2001; Taylor et al. 1996). The only disadvantage is the necessity to acquire separate spectra for each plane sampled.

## 13.2.3 Application

MRS is useful in diagnosing and assessing brain tumors because tumors usually have elevated Cho levels and subnormal NAA levels compared to normal brain tissue. A Cho/NAA ratio of ≥5 is strongly suggestive of tumor. These features are also found in other conditions in which membrane turnover is increased and the number of healthy, mature neurons is decreased (e.g., immature brain, some types of dysplastic brain, and inflammation). It is important to know the normal peak ratios in the region of brain being investigated. The concentration of NAA is normally 10 % lower in the cerebellum than in cerebral white matter (Usenius et al. 1995; Wang et al. 1995). Cho concentrations in the cerebellum and pons are 70 % higher than in other areas (Usenius et al. 1995). Increased Cho in relation to NAA is even more dramatic in neonates (Tzika et al. 1996). Ratios of metabolites can also differ in different regions of the brain, even within different portions of the cerebral cortex (Wang et al. 1995). Therefore, it is critical to correlate MRS with MRI and other tests in order to avoid false positive results suggestive of tumor, when the actual process is another diagnosis (Sutton et al. 1992).

Once the diagnosis of tumor is established, MRS can be of some use in grading astrocytic neoplasms. In general, the farther the metabolite peaks vary from normal, the more likely that the tumor is aggressive (Hunter and Wang 2001). In particular, the Lac peak magnitude tends to be more elevated in more aggressive neoplasms (Girard et al. 1998). It should be noted, however, that juvenile pilocytic astrocytomas, among the most benign of brain tumors, have elevated choline and lactate, along with reduced NAA (Lazareff et al. 1999). In addition, similar grades of tumors of different histologic type may have very different spectra (e.g., a low-grade oligodendroglioma may have a very different spectrum from a low-grade astrocytoma). For these reasons, grading of neoplasms based on MRS has

focused on determining peak magnitudes and ratios in tumors of the same histologic type (Poptani et al. 1995; Shimizu et al. 1996; Tzika et al. 1996; Chang et al. 1998; Horska et al. 2001), and even in these cases, it is not entirely reliable (Kimura et al. 2001; Lazareff et al. 1999; Tzika et al. 1996, 1997; Chang et al. 1998; Barker et al. 1993; Shino et al. 1999).

Rarely, tumors have unique spectra that can help narrow the differential diagnosis from what is derived from routine MR imaging alone. For example, meningiomas and central neurocytomas exhibit an alanine peak that is typically not found in other neoplasms. In these two tumor types, it may represent a secondary marker for more aggressive histology (Kinoshita and Yokota 1997; Krishnamoorthy et al. 2007; Kugel et al. 1992; Lehnhardt et al. 2001). An elevated taurine peak has been preferentially discovered in medulloblastomas, which is not the case for astrocytomas within the posterior fossa (Chawla et al. 2007; Moreno-Torres et al. 2004). The combination of prominent Cho, Lac, and lipids peaks, and minimal NAA peaks, and basically absent myoinositol peaks has been described with atypical teratoid rhabdoid tumors (Bruggers and Moore 2014). Citrate has been observed in pediatric brain tumors, particularly diffuse intrinsic brain stem gliomas, although also in the developing brain of infants younger than 6 months (Seymour et al. 2008).

MRS can be helpful in selecting the best biopsy site in heterogeneous neoplasms (Dowling et al. 2001; Martin et al. 2001). However, for MRS to be useful in this regard, the voxel size must be small compared to the size of the neoplasm. Spectroscopic data obtained from a given volume of brain represents the average of the metabolic components of the volume. If the voxel is large or the tumor is small, the voxel might contain regions of both high and low-grade tumor, normal brain, and necrosis (Tzika et al. 1996). The resultant spectrum reflects the percentage of each component and does not reflect the nature of the tumor. For example, the MRS of a highly aggressive neoplasm with a large component of necrosis or normal brain or low-grade tumor could mimic the spectra of a low-grade neoplasm (Sijens et al. 1995; Venkatesh et al. 2001). Because spectra can also be contaminated

by adjacent CSF or by fat from the calvarium or scalp (Hunter and Wang 2001; Norfray et al. 1999; Wang et al. 1996a; Sijens et al. 1995), it is imperative to use as small a voxel as possible. However, sampling many different voxels during a single exam necessitates excessively long scan times if each voxel is acquired separately. In order to reduce acquisition time, 3D MRSI can be used to sample a large volume of brain during a single acquisition, with small areas within the volume analyzed during the postprocessing step.

Although MRS can clearly distinguish abnormal from normal brain tissue, it does not always correctly differentiate a neoplasm from other disorders (Kim et al. 1997; Sutton et al. 1992; Wilken et al. 2000), particularly those with a high concentration of inflammatory cells (Venkatesh et al. 2001; Krouwer et al. 1998). There are many examples of inflammatory disorders, such as demyelinating plaques, tuberculomas, xanthogranulomas, HIV encephalitis, and HSV encephalitis, that have MRS features nearly identical to neoplasms (Venkatesh et al. 2001; Krouwer et al. 1998; Butzen et al. 2000; Shukla-Dave et al. 2001). These other processes should always be considered, particularly when the patient's history or imaging features are not consistent with a CNS tumor.

MRS can be useful in differentiating pyogenic abscess from tumor. Increased glycolysis and fermentation by bacteria produce elevated levels of lactate, acetate, and succinate, while proteolysis by enzymes produces valine, isoleucine, and leucine (Kim et al. 1997; Chang et al. 1998; Gupta et al. 2001). These compounds have protons that precess in the aliphatic region, upfield from NAA. Although elevated lactate and succinate associated with radiation necrosis makes MRS nonspecific in the posttherapy patient (Kim et al. 1997; Yeung et al. 2001), the presence of these peaks seems rather sensitive (92–100 %) and specific when MRS is performed at presentation (Kim et al. 1997; Kimura et al. 2001; Shukla-Dave et al. 2001; Gupta et al. 2001; Grand et al. 1999).

Distinguishing posttherapy injury from recurrent or residual neoplasm has been difficult using anatomic imaging techniques, as the enhancement and edema seen with the two conditions can be nearly identical. This distinction is pivotal, as earlier recognition of recurrence can prolong survival

or guide future treatment (Shtern 1992). MRS can be a useful technique in making this distinction, as an injured brain produces a different spectrum than a normal brain or tumor (Kamada et al. 1997). Early radiation injury produces elevated Cho from plasma and intracellular membrane disruption, but this usually clears quickly and a normal NAA peak remains (Szigety et al. 1993). A global decrease in peak amplitudes (NAA, Cho, and Cr peaks) is con-sistent with treatment injury without active neo-plasm (Kimura et al. 2001; Yousem et al. 1992; Ott et al. 1993; Tzika et al. 1997; Taylor et al. 1996). Recurrence is suggested by new or persistent ele-vation of Cho and reduction of NAA (Fig. 13.1) (Lazareff et al. 1999; Tzika et al. 1997; Sijens et al. 1995). MRS has also helped in determining survival, which can impact treatment stratification. High glutamate has been reported to be predictive
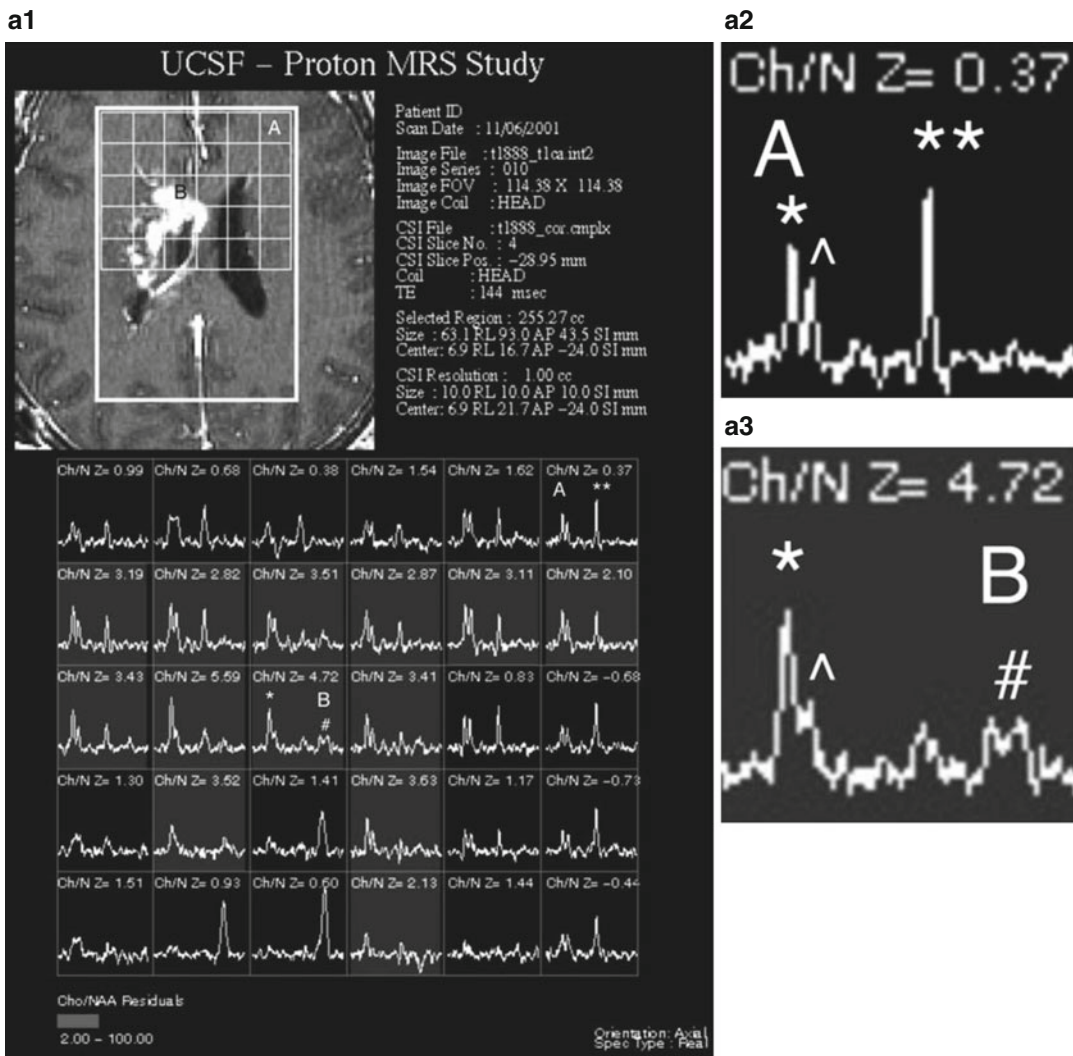


**Fig. 13.1** High-grade glioma with both improved spectra and anatomic imaging after receiving radiation therapy. (**a1**–**a3**) Pretreatment 3D chemical shift imaging (CSI) transposed on T1-weighted gadolinium-enhanced axial image. Spectrum voxel labeled *A* is within normal left frontal white matter; choline (*), creatine (^), and NAA (**) peaks are normal for age and location. Spectrum voxel labeled *B* is within enhancing neoplasm; the spec-trum shows elevated choline and lactate/lipid (#), with decreased NAA in the right genu. (**b1**–**b3**) Follow-up 3D CSI in the same location as image a. Choline peak (*) has decreased since the prior study, resulting in an improved *Z*-score, yet still has evidence of residual neoplasm. Spectrum voxel labeled *C* shows necrosis; all metabolites are decreased
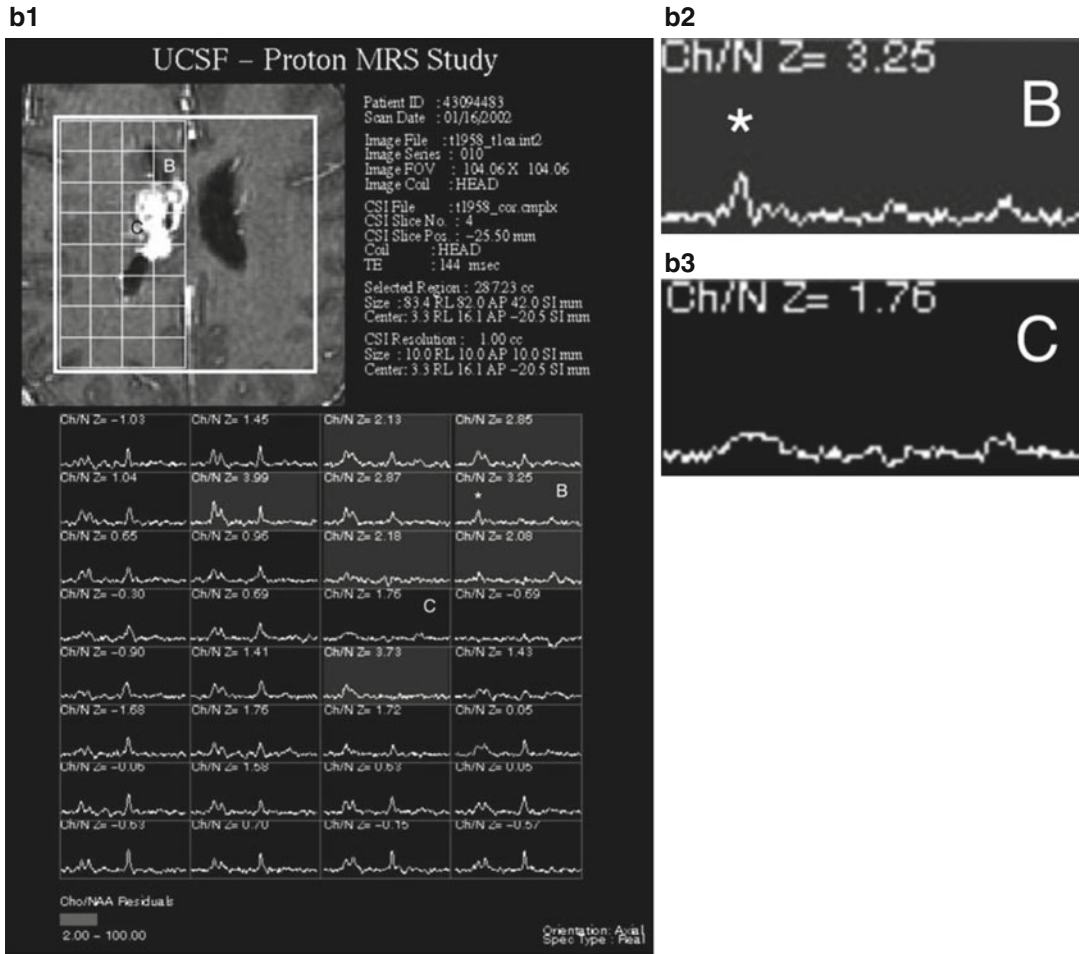
**b1**



**b2**



**b3**



**Fig. 13.1** (continued)

of poor survival in patients with medulloblastomas (Wilson et al. 2014).

There is no consensus as to how often patients should be evaluated. We believe that the most sensitive method to evaluate treatment efficacy and to screen for early recurrence or residual neoplasm is to perform serial exams, which allows comparison with a known baseline prior to treatment (Lazareff et al. 1999; Nelson et al. 1997a, 1999; Norfray et al. 1999; Vigneron et al. 2001). It is important to remember that, although combining MRS with MR imaging is more sensitive than MR imaging alone, sensitivity is not 100 %. A necrotic neoplasm with a paucity of viable tumor cells can have identical spectra to posttreatment necrosis (Taylor et al. 1996) this can

only be differentiated when the Cho increases on subsequent exams. Serial follow-up studies are, therefore, essential to detect early growth of residual neoplasm.

MRS is a promising tool for assessing pediatric patients with brain tumors. In the appropriate setting, spectroscopy can improve the delineation of neoplastic brain involvement, increase specificity of diagnosis, and help discriminate posttreatment injury from residual neoplasm. Research continues to define the role of MRS in grading neoplasms and possibly predicting treatment response (Lazareff et al. 1999; Waldrop et al. 1998; Tzika et al. 2001; Girard et al. 1998; Lin et al. 1999; Negendank et al. 1996).

## 13.3   MR Perfusion

### 13.3.1   Principles

Cerebral perfusion is defined as the delivery of nutrients and oxygen, via the blood, to brain tissue per unit volume. This is typically expressed in units of milliliters per 100 g of parenchyma per minute (Cha et al. 2002). With recent advances in fast imaging techniques and computer technology, it is now possible to capture the dynamic changes in cerebral perfusion using MR imaging. Perfusion MR imaging (pMRI) provides information on cerebral hemodynamic parameters that are reflective of tissue perfusion, including relative cerebral blood volume (rCBV), cerebral blood flow (CBF), and mean transit time (MTT).

pMRI has evolved from a research tool into a clinically useful technique due to wider availability of high-performance MR gradients that allow faster imaging sequences (e.g., echo planar imaging (EPI)) and improvement in computer image processing algorithms. Quantitative analysis of perfusion parameters can now be derived from a clinically useful volume of brain using MR perfusion. This technique takes us one step closer to evaluating intracranial pathophysiology, in addition to the anatomical information gathered from conventional MR. A brief review of pMRI is presented to better understand the methodology and the basis for clinical application of MR perfusion.

### 13.3.2   Technique

Several methods can be used to derive perfusion parameters using MR imaging. pMRI can be performed using either exogenous (gadolinium, deuterium oxide) contrast agents or endogenous (arterial water) (Cha et al. 2002).

Dynamic susceptibility-weighted contrast-enhanced perfusion MR imaging (DSC-pMRI) exploits the signal changes (T2* signal loss) during bolus passage of a contrast agent through the cerebral vessels (Aronen et al. 1994; Ball and Holland 2001; Cha et al. 2000a; Ludemann et al. 2000; Siegal et al. 1997; Strong et al. 1993). Using tracer kinetic principles, the signal change is converted to an integral of tissue contrast agent concentration (Peters 1998; Rosen et al. 1990; Weisskoff et al. 1994). These values are then used to generate perfusion maps of various hemodynamic parameters.

To successfully image a large volume of brain during the finite time that contrast is within the cerebral vessels, faster imaging methods are necessary. EPI fulfills this requirement, with a temporal resolution of 100 ms/slice. Several different pulse sequences can be used with EPI (e.g., spin echo, gradient echo). Spin echo images are thought to be more sensitive to signal changes from contrast agent within the intra-capillary volume (Weisskoff et al. 1994). Gradient echo images are more sensitive to medium to large vessels, and therefore greater signal drop is seen during the first pass of a contrast agent. Although more prone to susceptibility artifact, gradient echo techniques are more sensitive to small changes in blood volume. Therefore, the gradient echo technique does not require high doses of contrast agent as does spin echo to produce diagnostic images (Hunter and Wang 2001; Yeung et al. 2001; Cha et al. 2002).

Dynamic contrast-enhanced (DCE) perfusion MR imaging is another type of pMRI using gadolinium based contrast agent. In contrast to the first-pass effect of DSC-pMRI, DCE-pMRI exploits the steady-state hemodynamics of intravascular contrast agent to measure alterations in endothelial permeability, which can be used as a noninvasive marker of vascular leakiness and degree of tumor angiogenesis. DCE-pMRI is based on the acquisition of serial T1-weighted images before, during, and after contrast administration. In contrast to routine post-contrast images that reflect enhancement characteristics at a single time point, DCE perfusion depicts the wash-in, plateau, and washout contrast kinetics of the tumor (Cha 2006; Essig et al. 2013).

Arterial spin labeling (ASL) permits evaluation of CBF without the use of intravenous contrast. ASL uses arterial blood water as an endogenous tracer by inverting the magnetization of blood using radiofrequency pulses. After a brief delay to allow these "labeled" intravascular protons to flow into the brain, imaging of the brain is performed in order to see the degree of

flow of labeled protons into the cerebral hemispheres. Separate control images are also acquired in the same imaging session, and the signal difference between control and labeled images provides a measure of perfusion by arterial blood (Golay and Petersen 2006).

At our institution, ASL is performed on 1.5 T or 3 T field-strength scanners. While various methods of labeling were used in the early applications of ASL, the SNR of pseudocontinuous labeling is the method of choice for clinical applications (Zaharchuk 2012). We use a labeling period of 1,500 ms, followed by a 1,500 ms post-label delay. 3D images are obtained while suppressing background with fast spin echo stacked technique. The total image time for the ASL sequence is approximately 3–4 min.

### 13.3.3 Applications

DSC-pMRI, as adjunct imaging to conventional MR imaging, has several potential applications. With the wide availability and application of faster imaging hardware and software, DSC-pMRI can be incorporated into the routine evaluation of intracranial lesions. Clinical roles for DSC-pMRI include grading neoplasms, distinguishing high-grade primary neoplasm from single metastases, directing stereotactic biopsies, and distinguishing therapy-related brain injury from residual or recurrent tumor (Cha et al. 2002; Knopp et al. 1999; Law et al. 2002; Maeda et al. 1993; Tzika et al. 2002). Some advocate that DSC-pMRI may be helpful in adjusting chemotherapy dosing (Cha et al. 2000b).

Preliminary results on grading of gliomas with DSC-pMRI are promising. Although some authors using spin echo sequences have shown no statistical correlation between tumor grade and perfusion imaging, gradient echo-derived blood volumes have been more robust in distinguishing grades of glioma (Aronen et al. 1994; Ball and Holland 2001; Ludemann et al. 2000; Roberts et al. 2000a; Rosen et al. 1991; Sugahara et al. 1998).

Separating high- from low-grade gliomas by histology relies on the presence of neovascularity

and necrosis (Giannini and Scheithauer 1997; Plate and Mennel 1995). DSC-pMRI is a method that can noninvasively assess tumor vascularity and is complementary to histopathology in determining the grade and malignancy potential of a neoplasm (Fig. 13.2) (Gerlowski and Jain 1986).

Histology alone may not accurately predict tumor biology or patient prognosis. DSC-pMRI correlates with the degree of tumor angiogenesis and therefore may be able to predict aggressive biology (Aronen et al. 1994). Hence, the more aggressive the tumor, the larger the rCBV, presumably due to tumor angiogenesis (Knopp et al. 1999; Sugahara et al. 1999). This technique offers a potentially powerful and noninvasive means of assessing tumor biology and serially monitoring changes in the tumor during therapy.

Most published reports using DSC-pMRI for tumor grading have studied adult patients. Sensitivity for this technique may be reduced in children since certain benign tumors, such as pilocytic astrocytoma and choroid plexus papilloma may have increased vascularity; that is, high rCBV (Ball and Holland 2001; Strong et al. 1993; Giannini and Scheithauer 1997; Plate and Mennel 1995; Keene et al. 1999). DSC-pMRI should be interpreted cautiously in heterogeneous tumors since rCBV can vary depending on the location chosen to place the region of interest. A region of interest placed in an area of necrosis or nonaggressive portion of the neoplasm could erroneously underestimate rCBV and result in undergrading of tumor. Alternatively, cortically based neoplasms that are contiguous with the brain surface vessels may be falsely given a higher grade due to a high rCBV from a region of interest placed over vessels (Sugahara et al. 2001). Larger studies are needed prior to DSC-pMRI's inclusion as a routine clinical practice for grading tumors in children.

A promising application of perfusion imaging is distinguishing treatment-induced brain injury from residual or recurrent neoplasm (Cha et al. 2000b, 2002; Siegal et al. 1997; Roberts et al. 2000a; Rosen et al. 1991; Sugahara et al. 1999). With routine MR imaging, both entities can enhance after contrast administration and are indistinguishable until growth on serial imaging
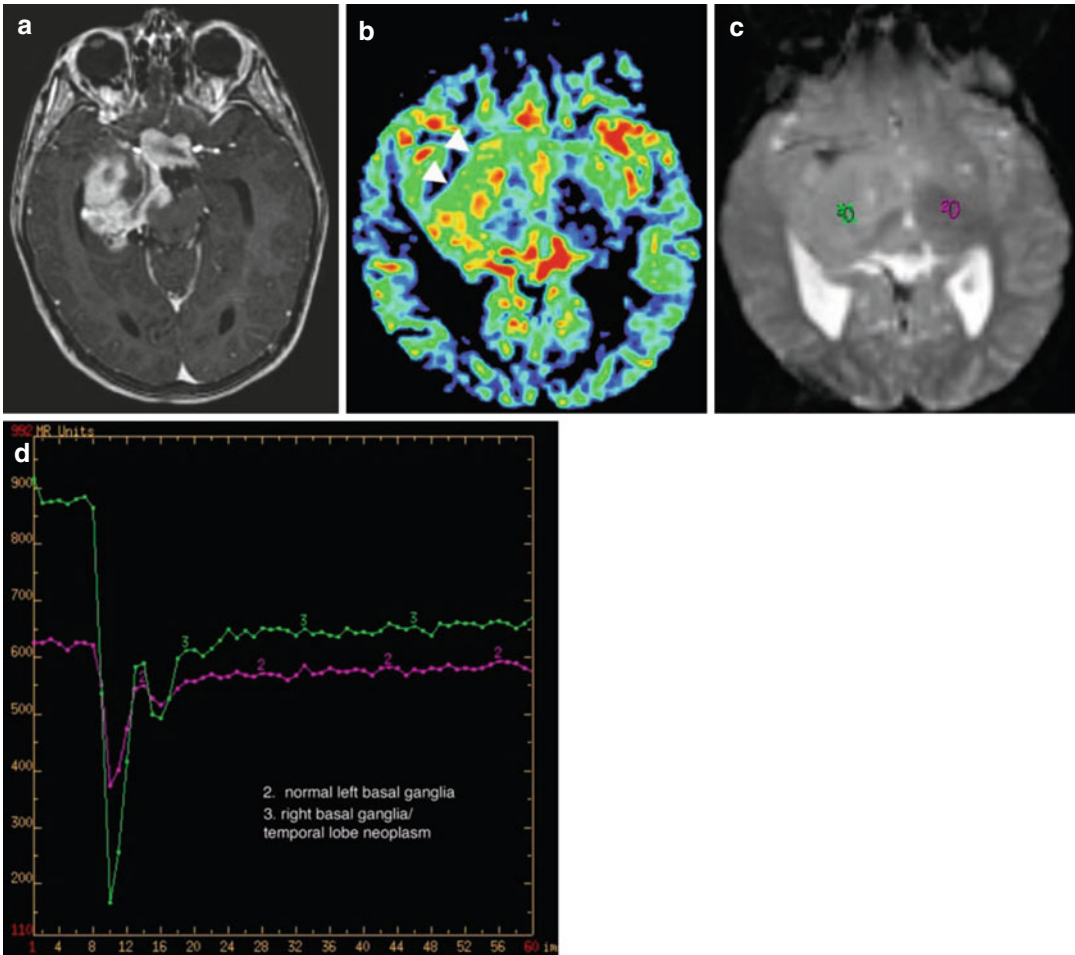
**Fig. 13.2** Right medial temporal lobe and chiasmatic glioma with pMR imaging characteristics of a vascular, intra-axial neoplasm. (**a**) Axial T1-weighted gadolinium-enhanced image of the infiltrating, enhancing neoplasm. (**b**) Axial color map of the relative cerebral blood volume (CBV) showing increased CBV within the neoplasm (*white arrowheads*) relative to normal vascularity on the contralateral side. (**c**) Axial T2-weighted image shows the regions (*ovals*) that were sampled to calculate the time-signal curves (*2* normal left basal ganglia, *3* neoplasm). (**d**) Time-signal curve shows an intact blood–brain barrier (BBB) in region *2* (normal recovery of signal after the passage of the contrast bolus) but a partially disrupted BBB in region *3* (slower, incomplete recovery after the bolus due to contrast leaking through the BBB)

favors a diagnosis of neoplasm. DSC-pMRI takes advantage of the pathophysiologic differences in vascularity to separate the entities. Posttreatment brain injury, in part, is believed to be the result of endothelial damage followed by vascular thrombosis and blood–brain barrier (BBB) breakdown. This ultimately leads to hypoperfusion of the affected tissue (Chan et al. 1999). The final common pathway of delayed radiation injury is vascular thrombosis and fibrinoid necrosis, which on DSC-pMRI manifests as a decrease in rCBV when compared to normal tissue (Cha et al. 2000b, 2002). On the other hand, tumor cells require a viable blood supply for growth and spread and, therefore, increased rCBV is seen in recurrent and residual neoplasms (Ball and Holland 2001; Cha et al. 2000b; Plate and Mennel 1995). Preliminary results show that decreased signal on DSC-pMRI correlates well with treatment-induced brain injury (Ball and Holland 2001; Cha et al. 2000b; Plate and Mennel 1995).

Exceptions still exist in making this important distinction between tumor and therapy-induced brain injury. Normal or even decreased rCBV in the area of residual tumor can occur if neoplastic tissue is mixed with hypovascular necrotic tissue. Treatment-induced injury can lead to aneurysmal dilation of vessels and formation of telangiectasias that can artificially elevate the rCBV, leading to false positive results. Petechial hemorrhage or calcification in an area of residual tumor can produce susceptibility artifact that artificially reduces the rCBV, resulting in a false negative result (Sugahara et al. 2000). Further research is needed prior to standardized clinical use throughout multiple institutions.

DSC-pMRI continues to be investigated for use in guiding stereotactic biopsy of intracranial neoplasms. Usually, CT and MRI-guided biopsies of brain tumors, are directed to areas of conventional contrast enhancement. This approach, however, is prone to sampling error due to the intrinsic limitations of imaging enhancement to detect the most aggressive portion of a tumor (Cha et al. 2002; Joyce et al. 1978). In addition, limited tissue sample size can lead to erroneous grading and inadequate evaluation (Cappabianca et al. 1991; Chandrasoma et al. 1989).

Contrast enhancement on MR images reflects the areas of breakdown within the BBB (Greenwood 1991). This is often in the rim adjacent to a necrotic portion of the neoplasm. Elevated rCBV is considered to represent the areas of vascular hyperplasia in the aggressive, viable neoplasm and may not always correspond to a contrast enhancing portion (Cha et al. 2002). Using DSC-pMRI in addition to conventional anatomical images could result in reduced false negatives and errors in assessing tumor grade. Although still investigational, DSC-pMRI may be helpful in localizing the most aggressive portion of a neoplasm and serve as a complimentary tool to anatomic imaging (Aronen et al. 1994; Knopp et al. 1999; Rosen et al. 1991).

Future applications for DSC-pMRI under development include mapping dose distributions in neoplasms and following perfusion maps for therapy-outcomes research for new therapeutic agents (Cha et al. 2000b, 2002; Ludemann et al. 2000; Roberts et al. 2000a).

DCE-pMRI permits quantitative assessment of the blood–brain barrier and microvascular permeability. This can provide a more thorough assessment of brain tumor angiogenesis. Another advantage of DCE-pMRI is the high SNR that allows imaging at a higher temporal and spatial resolution.

ASL of tumors can be easily assessed qualitatively as elevated CBF will manifest as hyperintense signal relative to the remaining brain, and decreased CBF will show hypointense signal. For absolute measurements, regions of interests are placed on the tumor using postprocessing software. Comparisons can be made relative to the remaining brain or other areas within the tumor. Using the aid of conventional MRI sequences, care is taken to avoid placing regions of interest within areas of cyst, hemorrhage, or necrosis. Maximum ASL signal is recorded, in keeping with other studies in the assessment of gliomas (Knopp et al. 1999; Sugahara et al. 2001). Distinguishing high-grade and low-grade tumors has been suggested using ASL technique (Yeom et al. 2014).

The advantages of ASL include the lack of contrast requirement, high SNR, labeling efficiency, and potential for absolute CBF quantification. ASL can be repeated in cases of patient motion. In children, immature paranasal sinuses contribute to improved image quality due to less artifact (Yeom et al. 2014).

In summary, pMRI is no longer primarily a research tool, but an important diagnostic tool complementing conventional anatomical imaging. Clinical use for tumor grading, differentiating between residual neoplasm and treatment-associated injury, and assisting in therapy dosing and treatment follow-up are on the horizon. Guiding biopsies within heterogeneous tumors by perfusion imaging may reduce sampling errors and improve diagnostic accuracy.

## 13.3.4 Limitations

DSC-pMRI has several important constraints. Sensitivity to susceptibility artifact prevents its use in brain adjacent to the paranasal sinuses or

the skull base (Cha et al. 2002; Ball and Holland 2001; Poussaint et al. 1995). The sequence is very sensitive to patient motion, and SNR is low in comparison to anatomic MR images (Cha et al. 2002; Aronen et al. 1994; Siegal et al. 1997). Only a limited volume of brain can be covered during the time it requires a contrast bolus to pass through the intracranial vasculature. Also, a compact delivery of the bolus (through a power injector) may be difficult to attain in a patient who has limited intravenous access (Siegal et al. 1997). Furthermore, care must be taken to recognize false positives that are created by normal structures (e.g., choroid plexus and cortical veins) (Aronen et al. 1994; Sugahara et al. 1998). Additional costs may be substantial, due to the stringent hardware and software requirements to acquire and process the MR data. Access to a physicist familiar with the MR technique is also beneficial for continued support (Cha et al. 2002).

DCE-pMRI is also not without limitations, which include the complexity in image acquisition and user-dependence. The postprocessing is also challenging, as the kinetics modeling and software both require some training (Essig et al. 2013).

Limitations to ASL include sensitivity to motion and artifact from metal in the face and head region from dental/orthodontic procedures. There may also be an underestimation of CBF in regions of delayed flow such as white matter (van Gelderen et al. 2008).

## 13.4   Nuclear Medicine

### 13.4.1   Principles

The role of radionuclide CNS imaging continues to evolve. The most commonly used techniques are single photon emission computed tomography (SPECT and positron emission tomography (PET)). Areas of current study include: differentiating lesions with similar imaging appearances (e.g., lymphoma from toxoplasmosis by thallium uptake), differentiating treatment injury from residual neoplasm, grading neoplasms, localizing the most aggressive portion of the tumor prior to therapy, predicting response to therapy, and local-

izing eloquent cortices prior to surgery (Maria et al. 1998; Ricci et al. 1998).

The most widely practiced application is that of differentiating residual neoplasm from treatment injury. Without special techniques (such as pMRI, see earlier section), this differentiation can be extremely difficult by conventional CT and MRI (Brunelle 2000; Di Chiro et al. 1988; Valk and Dillon 1991). Both entities produce altered vasculature that can result in identical-appearing edema and enhancement. Even biopsy can lead to a false diagnosis. It is difficult to know which area of enhancement represents an aggressive margin of neoplasm or just an area of active necrosis and BBB breakdown (Poussaint et al. 1995). If cognizant of the limitations, radionuclide imaging may be very helpful to select clinical scenarios.

Both SPECT and PET, utilizing several radionuclide imaging agents, have been studied in attempts to distinguish treatment injury from neoplasm. [99m]Technetium, [201]thallium, [18]fluorine, and [11]carbon agents are the most cited (Di Chiro et al. 1988; Dadparvar et al. 2000; Go et al. 1994; Kim et al. 1992; Maria et al. 1994; Ogawa et al. 1991; Shinoura et al. 1997). [201]Thallium SPECT and ^{18}F-fluorodeoxyglucose (FDG) PET are currently the most utilized methods, but additional promising radionuclides are on the horizon (Chen and Silverman 2008; Hatakeyama et al. 2008; Lorberboym et al. 1997; Maria et al. 1997). The remaining discussion is limited to these agents.

### 13.4.2   Mechanism and Technique

The mechanism of thallium sequestration within tumor cells is unknown. The most accepted theories propose either passive uptake over a potential membrane gradient or high affinity for potassium-activated adenosine triphosphatase (Kim et al. 1992; Kaplan et al. 1987). Alteration of the BBB also contributes (Kim et al. 1992). Whatever the mechanism, thallium seems to be incorporated into neoplastic glial cells considerably more than into nonneoplastic cells. A typical dose for a [201]thallium brain scan is 0.03–0.05 mCi/kg, and images are obtained 5–10 min after administering the dose intravenously (O'Tuama et al. 1998).

**Fig. 13.3** PET imaging complimenting anatomic MR imaging in a case of tumor recurrence. (**a**) Axial T1-weighted gadolinium-enhanced image of a tectal glioma at presentation. (**b**) Axial T1-weighted gadolinium-enhanced image of the same tectal glioma (*white arrow*) after radiation treatment. The enhancing mass may represent posttreatment granulation tissue or residual neoplasm. (**c**) Axial PET image showing increased activity (*black arrow*) within the tectal mass, indicating residual active neoplasm
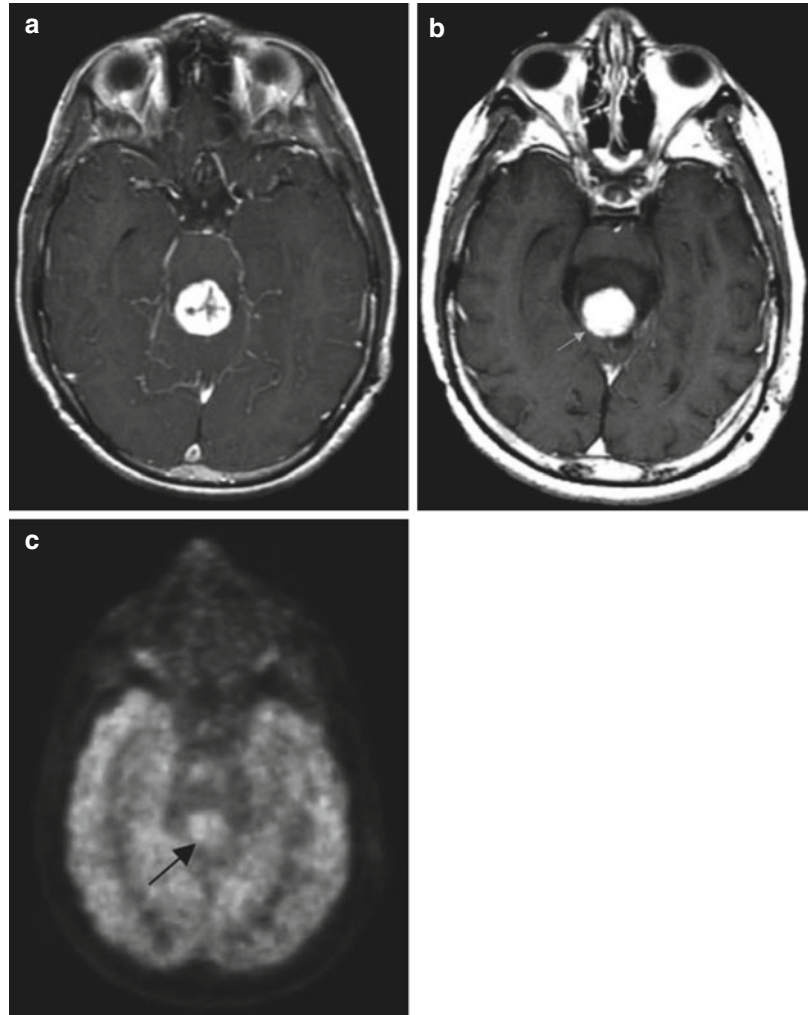


PET imaging for brain tumors is primarily with $^{18}$FDG, a compound that has chemical properties similar to glucose and is therefore incorporated into astrocytes as an energy source. However, $^{18}$FDG cannot be normally metabolized and, therefore, becomes entrapped within cells (Wang et al. 1996b). Increased $^{18}$FDG within tumor cells is attributed to the increased rate of glycolysis in rapidly growing neoplasms (Shinoura et al. 1997; De Witte et al. 2000). For pediatric brain scans, 0.14 mCi/kg of $^{18}$FDG is given intravenously and images are usually obtained 30 min later (Kaplan et al. 1999; Kincaid et al. 1998).

More recently, $^{18}$F-fluorothymidine ($^{18}$FLT) and $^{11}$C-thymidine (TdR) have shown promise as alternatives to $^{18}$FDG for the evaluation of brain tumors in adult patients and animal models. These agents may more accurately reflect tumor-cell biology, owing to their interaction with thymidine kinase 1 (TK1), which is preferentially expressed during the S-phase of the cell cycle in proliferating cells. Intracellular phosphorylation of these agents by TK1 results in their retention within tumor cells. In addition, the near absence of proliferating cells in normal brain results in increased conspicuity of tumor from background with these agents. The higher cortical background activity of $^{18}$FDG results in a relatively lower sensitivity to distinguish between normal tissue and brain tumor cells (Hatakeyama et al. 2008; Bradbury et al. 2008; Muzi et al. 2006; Ullrich et al. 2008).

O-(2-18F-fluoroethyl)-L-tyrosine (^{18}F-FET) has been recently evaluated in children and adolescents with brain tumors with promising results (Dunkl et al. 2015), although only limited data exist. ^{18}F-fluoromisoidazole is an agent sensitive to detecting hypoxia and is being studied as hypoxic regions within tumor are intrinsically more resistant to both chemotherapy and radiotherapy (Puttick et al. 2014).

### 13.4.3 Applications and Limitations

The usage of PET and SPECT to distinguish tumor from posttreatment injury has been studied extensively (Fig. 13.3). Both sensitivity and specificity of [18]FDG PET are in the range of 80–90 % (Di Chiro et al. 1988; Valk and Dillon 1991; Kim et al. 1992; Pujol et al. 1998). At least 80 % of pediatric tumors have a high affinity for thallium. It may therefore be useful to distinguish neoplasm from posttreatment granulation tissue (Maria et al. 1998; Brunelle 2000). However, the grade of the neoplasm and histologic type do not always correlate with the amount of thallium uptake (Maria et al. 1994). Pilocytic astrocytoma has a very high metabolic rate and therefore often a high radiotracer uptake, even though it is a relatively benign neoplasm.

The data for PET are calculated from lesions that are at least 5–7 mm in dimension, the lower limits of resolution for this modality. This imposes a limitation on early detection of subtle neoplastic recurrence. Furthermore, the percentage of false negatives is rather high and, as a result, many authors do not consider this method acceptable for making therapeutic (Kim et al. 1992; Ogawa et al. 1991; Barker et al. 1997; Valk et al. 1988). Other PET agents, such as FLT, TdR ^{11}C-methionine, ^{11}C-choline, and ^{11}C-tyrosine, have either had limited success in detecting neoplastic recurrence or are under active investigation (Go et al. 1994; Shinoura et al. 1997; Hatakeyama et al. 2008; Pirotte et al. 2007). The 20-min half-life of ^{11}C agents necessitates on-site production, which is an obstacle to widespread use.

Biopsy guidance by PET has been successful in the limited number of patients studied (Go et al. 1994; Pirotte et al. 2007; Massager et al. 2000). In theory, the most aggressive portion of a tumor has the highest glucose uptake and, thus, the highest [18]FDG uptake; thus, the PET can assist in localizing the most aggressive portion of a heterogeneous neoplasm for proper staging. However, identification of the most aggressive portion of the tumor has not been reproducible at every institution. This may be due to difficulties in coregistering the PET images to anatomic imaging (e.g., MR imaging) and, perhaps, a result of the difficulty in identifying very small regions of high-grade tumor (Maria et al. 1994, 1998). Furthermore, it can be difficult to differentiate regions of cortex (which has higher [18]FDG uptake compared to normal white matter) from regions of tumor recurrence without additional MR imaging.

The thymidine radionuclides do not suffer from this high background activity. Yet, analysis of uptake kinetics for thymidine tracers offers conflicting results as to their utility in assessing tumor proliferation (Muzi et al. 2006; Ullrich et al. 2008). Localizing the most aggressive portion of the tumor with thymidine agents has been most successful with suspected high-grade, untreated gliomas (Muzi et al. 2006).

Accurately predicting tumor grade by imaging is imprecise and remains an elusive goal in practice. Some authors claim that radionuclide imaging is an equivalent, or occasionally better, predictor of survival in patients with a malignant glioma compared with the prediction based on histologic grade (Valk et al. 1988). Others believe that PET is at least adequate to distinguish high- from low-grade brain neoplasms (Valk and Dillon 1991; Kincaid et al. 1998; Pirotte et al. 2007; Black et al. 1994; Provenzale et al. 1999). However, most results indicate that nuclear imaging does not grade brain neoplasms with adequate accuracy to make it useful in clinical practice (Hatakeyama et al. 2008; O'Tuama et al. 1998; De Witte et al. 2000; Muzi et al. 2006; Choi et al. 2000). For example, high-grade neoplasms, often necrotic in part, have low uptake in the necrotic regions so that when averaged with high-uptake regions, they may appear as low-grade neoplasms when calculating overall uptake. In addition,

some low-grade pediatric neoplasms, such as pilocytic astrocytomas have increased uptake, making them appear to be high-grade neoplasms.

Another potential application of radionuclides is to identify tumors that are sensitive to anti-angiogenic agents (O'Tuama et al. 1998; Valk et al. 1988). Some authors suggest using PET to localize eloquent cortices preoperatively for patients unable to tolerate MR imaging (Kaplan et al. 1999).

In general, radionuclide imaging is infrequently used for pediatric brain neoplasms at UCSF, with conventional MR imaging, perfusion imaging, and magnetic source imaging (MSI) being the imaging tools of choice. Radionuclide imaging also imposes a significant radiation dose, which is a significant issue in the pediatric population, as the effects of radiation exposure to children have a longer time to develop, with a resulting increase in its potential effects (Mettler et al. 2008). Each institution should determine the optimal tools for their patients depending upon their equipment and individual strengths.

One area of growing research is the use of combined PET-MRI via single modality scanning in the assessment of adult brain tumors (Puttick et al. 2014). PET-MRI scanners have improved temporal and spatial coregistration as opposed to scanning separately. In addition, the combined use will help validate the other modality. Our institution is currently evaluating this new modality to determine if this combined role can provide benefit.

## 13.5 BOLD/MSI

### 13.5.1 Principles

Two techniques used for locating brain activity during specific tasks are blood oxygenation level-dependent (BOLD) imaging and MSI. Many clinical applications of these techniques are under investigation, including evaluating reorganization after injury and deterioration during progressive disease, evaluation of therapies, and cortical mapping prior

to neurosurgery (Roberts et al. 2000b; Vezina 1997). These techniques are well-developed in adults but are less useful in children, as they require a great deal of cooperation by the patient. Some authors have had success in children through the use of multiple training sessions. However, such training requires considerable time, personnel, and space, which are rarely available in most centers. Task-related activations, which require that the patient perform specific tasks, may be difficult or impossible in individuals with deficits such as reading disorders, mental retardation, hearing loss, and paralysis (Breier et al. 1999; Otsubo and Snead 2001; Simos et al. 1999). It is possible to perform some studies on sedated children, but it is not yet clear how much effect the sedation has on the results. Therefore, this section is based mainly on results in adults, in the hope that the difficulties in performing these studies in children will soon be overcome.

### 13.5.2 Mechanism of BOLD Imaging

In BOLD images, contrast is created by a local increase of oxygenated blood in activated tissue (Martin and Marcar 2001; Stippich et al. 1998). In theory, an activated group of neurons requires increased oxygenation. This increased need is fulfilled by local vasodilation, allowing more oxygenated blood to be transported to the activated cerebral cortex. The increase in blood flow more than compensates for the increased oxygen consumption, resulting in local increase in oxyhemoglobin and decrease in deoxyhemoglobin. As oxyhemoglobin is diamagnetic (does not alter the local magnetic field) and deoxyhemoglobin is paramagnetic (alters the local magnetic field and results in local signal loss), the reduced local concentration of deoxyhemoglobin results in less signal loss and increased local signal intensity (Beisteiner et al. 1995; Boxerman et al. 1995). This local signal alteration can be detected by susceptibility-weighted MR imaging sequences, if multiple acquisitions are performed.

## 13.5.3 Mechanism of MSI

Neuronal activation results in electrical current, which can be measured with electroencephalography. The electrical current generates magnetic flux, the magnitude of which is in the order of a few picoTeslas, a quantity that is 8 orders of magnitude smaller than that produced from the earth's magnetic field and 12 orders smaller than that produced from MR imaging (Alberstone et al. 2000; Lev and Grant 2000). When performed in a room shielded from external magnetic fields, superconducting quantum interference devices (SQUIDs) (Stippich et al. 1998; Ganslandt et al. 1999) can be used to measure and localize these minute neuromagnetic signals using small receivers placed on the scalp (Alberstone et al. 2000; Papanicolaou et al. 2001). This technique is known as magnetoencephalography (MEG). MEG signal is generated from intracellular electron flux, not local vascular changes (as seen with fMRI) (Roberts and Rowley 1997), distinguishing it from EEG, which detects extracellular currents and is therefore less precise than MEG (Alberstone et al. 2000). Superimposition of MEG data on colocalized MR images is referred to as MSI (Stippich et al. 1998).

## 13.5.4 Applications of BOLD and MSI

The most widely used clinical application of BOLD imaging and MSI is the localization of eloquent function in the brain for preoperative planning (Fig. 13.4) (Roberts and Rowley 1997; Disbrow et al. 1999). Both BOLD and MSI can accurately localize the primary motor cortex (Pujol et al. 1998; Roberts and Rowley 1997). Sensitivity varies from 82 to 100%, and often depends on whether the primary motor cortex is merely displaced, or partially destroyed by the pathologic process. Both techniques can also be used for localizing the language centers prior to surgical resection of neoplasm or of the temporal lobe for epilepsy (Simos et al. 1999). BOLD may have the additional benefit over MEG of simultaneously localizing multiple areas involved in complex brain function (Roberts et al. 2000b).

The definitive test used to localize motor cortex is intraoperative cortical surface recording (Suzuki and Yasui 1992). For identification of language centers in either the right or left cerebral hemispheres, the Wada test (intracarotid amytal test) has been the standard test for many years, but BOLD techniques have similar sensitivities and are less invasive.
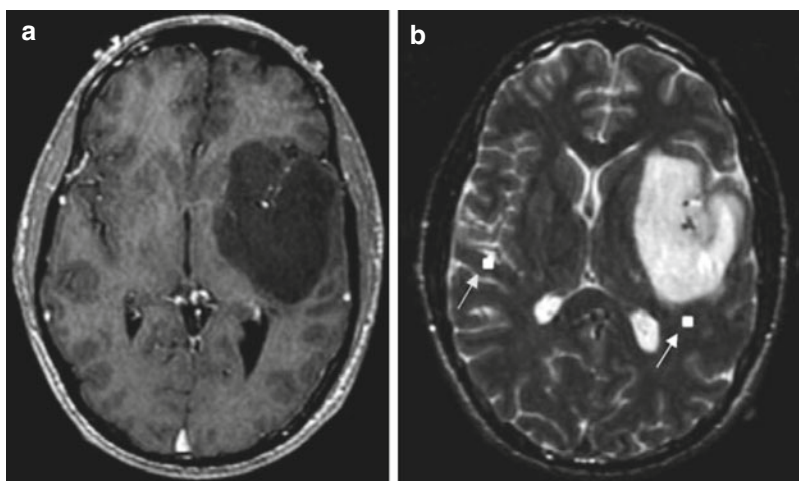
**Fig. 13.4** Magnetic source imaging for preoperative surgical planning in a patient who presented with grand mal seizure and aura but without speech or motor deficits. (**a**) Axial T1-weighted gadolinium-enhanced image showing a nonenhancing left temporal lobe/basal ganglia low-grade glioma. (**b**) Axial T2-weighted image showing white squares (*arrows*) that correspond to areas of auditory stimulation with a 1,000 Hz frequency tone. The auditory cortex on the left side is displaced, but not invaded, by the neoplasm

BOLD imaging has two major advantages in comparison to intraoperative surface recording: (1) localization is obtained preoperatively, allowing prospective surgical planning, and (2) the study can be performed at the same time as the preoperative MR imaging instead of lengthening operating room time for an additional procedure. Both techniques suffer when anatomic landmarks are distorted by the tumor, as the surgeon may encounter inadequate surgical exposure of the primary motor cortex, and the navigation based on the MR image may be changed by opening of the calvarium (Cedzich et al. 1996). Anesthetic agents may also influence the sensitivity of both the intraoperative and BOLD techniques (Cedzich et al. 1996), although older children and teens can generally undergo BOLD analysis without the need for sedation. In adults, overall sensitivity of intra-operatively localized eloquent function is roughly 91–94 % (estimated by postoperative deficits), which is similar to functional imaging (Simos et al. 1999; Ganslandt et al. 1999; Szymanski et al. 2001).

The Wada test requires an invasive catheter angiogram and sedation, both with inherent risks. Hemispheric dominance can be established in the majority of cases, but more specific cortical mapping is not possible (Simos et al. 1999). MSI and BOLD are both as sensitive and provide additional information that guides surgical approach and extent of resection (Pujol et al. 1998; Alberstone et al. 2000; Ganslandt et al. 1999; Dillon and Roberts 1999). MSI localizes eloquent regions of cerebral cortex, such as the primary motor cortex, within 3–4 mm in comparison to intraoperative electrocortical stimulation (Breier et al. 1999; Szymanski et al. 2001; Wheless et al. 1999).

### 13.5.5 Limitations

Several pitfalls must be kept in mind when implementing these new techniques. Limitations of BOLD imaging include poor temporal resolution that can never be better than the time that is required to produce a hemodynamic response to activated neurons, roughly 2–5 s (Martin and

Marcar 2001; Lev and Grant 2000; Roberts and Rowley 1997). The spatial resolution is dependent on the anatomic proximity of vessels to activated brain; high-signal contribution by sulcal veins has a marked negative effect on resolution (Roberts and Rowley 1997; Dillon and Roberts 1999; Holodny et al. 1999). Infiltration by neoplasm and edema can further distort the anatomic relationship and possibly alter the autoregulation of local vessels (Pujol et al. 1998; Dillon and Roberts 1999; Holodny et al. 1999). Motion artifact, larger caliber vessels, and inflow effects can further distort localization (Pujol et al. 1998; Beisteiner et al. 1995; Boxerman et al. 1995; Holodny et al. 1999; Field et al. 2000). Despite these shortcomings, BOLD generally localizes activated groups of neurons within 1–2 cm of their anatomic location.

MSI is hindered by susceptibility artifact from orthodontia and other ferromagnetic metals that cause overwhelming artifacts (Breier et al. 1999); BOLD imaging is also affected by such artifacts, but not as severely. The precision of labeling eloquent cortex by MEG is very good, but not perfect. Point localization is reduced by the inaccuracies of transposing data from MEG to MRI, by roughly 4 mm of dispersal (Szymanski et al. 2001). Overall error in localization is thought to be approximately 1 cm (Beisteiner et al. 1995). This is superior to other accepted techniques, including BOLD. The largest drawback of MSI is the cost and lack of availability of the necessary equipment; whereas BOLD can be performed on a clinical magnet with software upgrade, MSI requires an expensive neuromagnetometer in addition to a clinical magnet.

In summary, functional imaging has some potential for use in pediatric brain tumor patients, but a number of problems need to be overcome before these techniques will be used routinely.

## 13.6 Diffusion Imaging

### 13.6.1 Principles

Diffusion-weighted imaging (DWI) is a technique that relies on the fact the motion of

water molecules causes decreased signal on specially acquired MR images (Mitchell 1999). Also available are special types of DWI, known as diffusion tensor imaging (DTI) and high angular resolution diffusion imaging (HARDI), which allow both the net direction and the magnitude of water motion in a voxel to be determined. These techniques have applications in the assessment of brain tumors.

## 13.6.2 Technique

All diffusion techniques allow the calculation of net water motion in a volume of tissue. The mean diffusivity (MD) represents the average motion of all free water molecules in a voxel during the period of the MR data acquisition (Filippi et al. 2001; Inglis et al. 1999; Poupon et al. 2000).

DTI and HARDI are based upon mathematical probability functions that calculate the precise net motion characteristics of the water protons in the voxel; in other words, they give the probability that any molecule is moving in any direction at any velocity during the time of the imaging. If all the water protons are equally free to move in all directions, the motion is said to be isotropic. If water protons move predominantly in one direction more than others (due to restricted movement in some directions or accentuated movement in others), the motion is said to be anisotropic. In the normal brain significant anisotropy is seen in the white matter. Water motion is greatest along the long axis of the axon fascicle, parallel to the axons and the axoplasmic flow. Motion along the short axis is perpendicular to the axons in the fascicle, hypothesized to be primarily impeded by the cell membrane and hydrophobic myelin sheath. The characteristics of the motion can be displayed either as images or mathematically (Filippi et al. 2001; Gauvain et al. 2001; Melhem et al. 2000; Pierpaoli et al. 1996).

Fractional anisotropy (FA) and MD are measurements derived from the diffusion tensor that have been independently studied with brain tumor imaging. FA quantifies the magnitude of diffusion directionality and is hypothesized to reflect the degree of alignment of cellular structures within fiber tracts as well as their structural integrity. MD (also called average diffusivity or apparent diffusion coefficient) is a measure of mean molecular motion that is hypothesized to be affected by cellular size and integrity. These measurements are commonly displayed as quantitative color maps overlying the brain images using commercially available software.

## 13.6.3 Applications

Few applications of diffusion imaging have been implemented for the routine analysis of pediatric brain tumors. DWI is less sensitive than routine sequences for assessing the extent of tumor involvement (Stadnik et al. 2001). Distinguishing between high- and low-grade primary tumors using MD values can be challenging given overlap between the tumor types (Lam et al. 2002). Nonetheless, DTI is being studied to evaluate this differentiation by evaluating the loss of anisotropy (Gauvain et al. 2001). DWI has proved useful in the assessment of posterior fossa tumors (Koral et al. 2013). DWI alone is able to distinguish juvenile pilocytic astrocytoma from medulloblastoma with high certainty, with the latter showing reduced diffusion (Jaremko et al. 2010). Another area in which diffusivity measurements have been found to be helpful is in distinguishing between ring-enhancing tumors and pyogenic abscesses. In general, cystic tumors have increased water motion compared with surrounding brain, but pyogenic abscesses have reduced water motion secondary to protein content from bacteria and inflammatory cells (Fig. 13.5) (Gauvain et al. 2001).

Diffusion characteristics can also be helpful to distinguish between cystic and solid tumors. For example, differentiation between an arachnoid and an epidermoid cyst may be difficult by conventional MR sequences or CT. CSF freely moves in an arachnoid cyst and therefore is isointense to the CSF space on DWI. An epidermoid cyst, however, is gelatinous and therefore has diffusion characteristics similar to brain tissue (Gauvain et al. 2001).

A current area of research for the use of DWI in brain tumor patients is delineating postoperative

Fig. 13.5 Diffusion-weighted images used to help distinguish abscess from necrotic glioma. (**a**) Axial T1-weighted gadolinium-enhanced image showing a rim-enhancing, centrally hypointense brainstem lesion (*black arrow*). (**b**) Axial diffusion-weighted image at the same level showing increased diffusion within the central portion of the lesion (*white arrow*) consistent with a necrotic glioma. (**c**) Different patient. Axial T1-weighted gadolinium-enhanced image showing a deep right parietal ring-enhancing lesion (*white arrow*). (**d**) Axial diffusion-weighted image at the same level showing reduced diffusion within this lesion (*white arrow*) and adjacent ventricle (*gray arrow*) confirming that this was an abscess and not a neoplasm
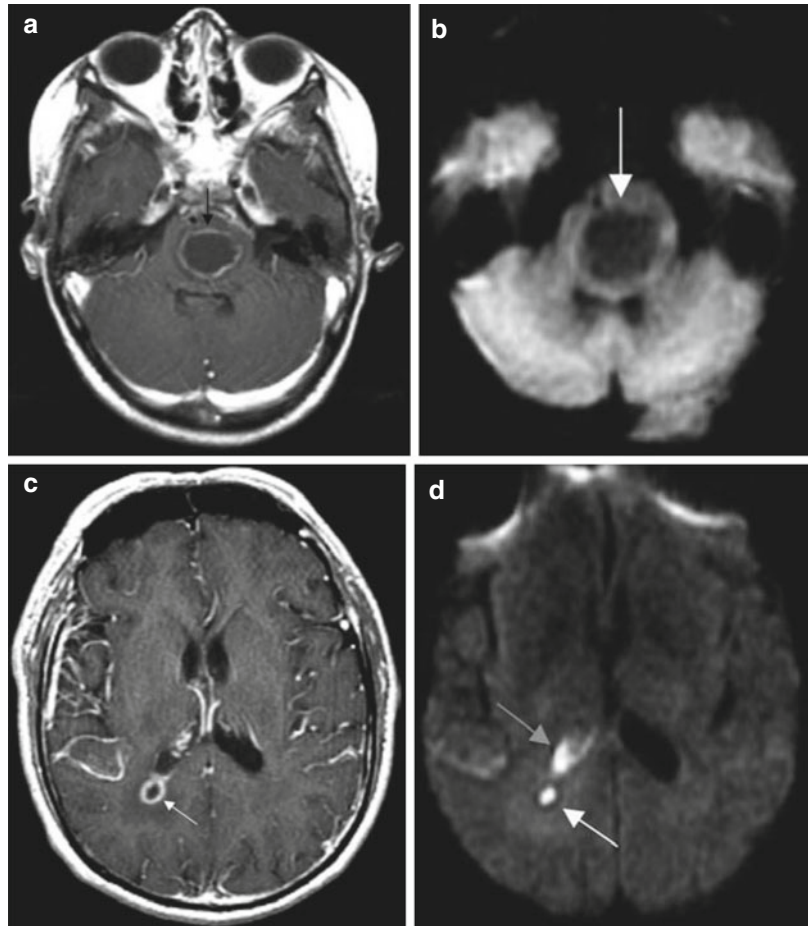


injury (Smith et al. 2005; Tanner et al. 2000). Acutely injured tissue generally has reduced diffusion for several days to weeks after the surgery. Nodular and fingerlike areas of reduced diffusion around the surgical cavity in the first few days after tumor resection likely represent tissue injury in the region of the resection (Fig. 13.6). Such areas will generally show marked enhancement from 2 weeks to 6 months after surgery and ultimately evolve to become astrogliosis or encephalomalacia. Mistaking this area of enhancement for recurrent tumor on the early postoperative scans could lead to unnecessary treatments that could adversely affect the patient (Smith et al. 2005). Therefore, analysis of the DWI on the early postoperative MRI scans is recommended to help determine whether new enhancement on later postoperative imaging is the result of perioperative injury versus recurrent tumor.

DTI can be used to identify specific white matter tracts within the brain, a technique referred to in the literature as tractography. Tractography is helpful in localizing large bundle white matter tracts, such as the corticospinal tracts, based on anatomic characteristics (Fig. 13.7). Knowledge of the location of these tracts, which can be shifted by mass effect from the tumor, can reduce postoperative morbidity and allows for more aggressive tumor resection, which has been shown to improve long-term survival (Keles et al. 2006; Smith et al. 2008).

Clinical applications of DWI for tumor assessment within the spine are limited. The poor spatial resolution, motion of the cord during the cardiac cycle, and the susceptibility effects from surrounding osseous structures prevent robust clinical use (Saritas et al. 2008). If surgical hardware is present within the spine, DWI will be further

**Fig. 13.6** Large chiasmatic and hypothalamic astrocytoma treated with partial surgical resection showing imaging evidence of postoperative ischemia. (**a**) Axial T1-weighted gadolinium-enhanced image shows the enhancing tumor preoperatively. (**b**) Axial T1-weighted gadolinium-enhanced image shows the postoperative resection cavity without evidence of residual enhancement. (**c**) Axial fluid attenuation inversion recovery (FLAIR) image of the resection cavity with thick posterolateral rim of high signal (*white arrow*) that may represent interstitial edema and/or injury. (**d**) Axial diffusion-weighted image at the same level shows high intensity (*arrows*), confirming that the area of increased signal on the FLAIR image was not edema, but postoperative ischemia
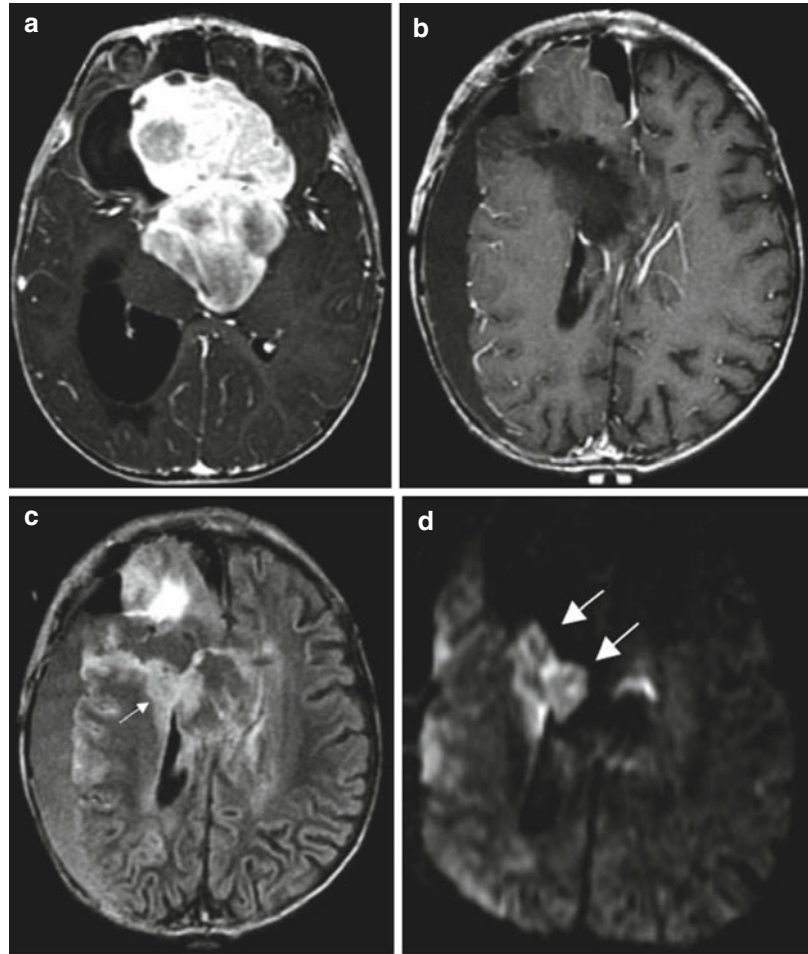


degraded. For these reasons, clinical applications of DWI for spinal cord tumors are infrequent. One study has described DWI to be used in conjunction with contrast-enhanced images for the assessment of spinal drop metastases (Hayes et al. 2012). Spinal DWI remains an area of active research, but with applications to neuro-oncology in the near future.

One last application of DTI and DWI is determination of prognosis. With respect to diffuse brain stem gliomas, patients with tumors displaying higher diffusivity and more isotropic diffusion tend to live longer (Chen et al. 2010), with the possible exception of optic pathway gliomas, where one study reported that higher ADC values correlated with earlier tumor progression (Yeom et al. 2013). In summary, diffusion-weighted sequences have several promising applications in pediatric brain tumor imaging that are under active investigation and will have an expanded role in the future.

## 13.7 Susceptibility-Weighted Imaging

### 13.7.1 Principles

Susceptibility weighted imaging (SWI) is a high-spatial resolution 3D gradient-echo MR technique that exploits the magnetic susceptibility differences of various tissues to yield a loss of signal. While SWI is sensitive to many compounds that distort the local magnetic field, detection of iron (primarily from blood products) and calcium are the primary roles in clinical imaging.
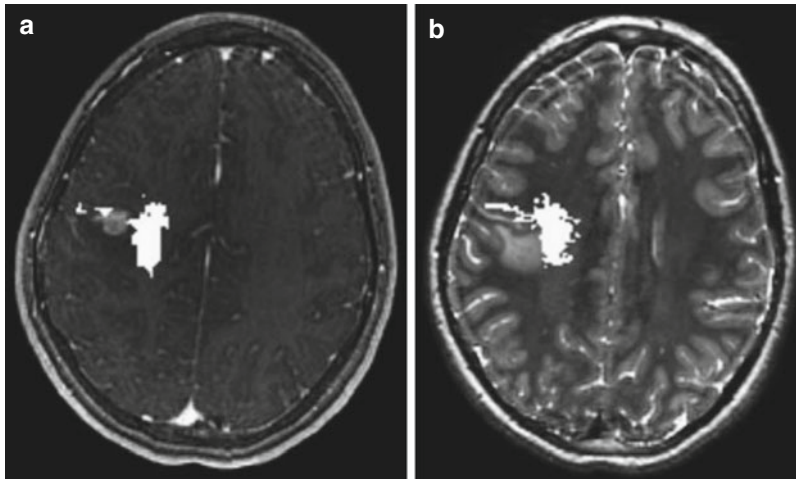
**Fig. 13.7** Small ganglioglioma within the postcentral gyrus presenting with left-arm seizures. (**a**) Axial 3D Spoiled Gradient Recalled (SPGR) gadolinium-enhanced image shows the corticospinal tracts medial to the enhanc-

ing tumor by diffusion tensor imaging (DTI) fiber tracking. The fiber tracts are overlaid on the anatomic images. (**b**) Axial T2-weighted image at the same level showing a similar relationship

## 13.7.2 Technique

Application of a magnetic field to the brain generates an induced field that varies with the magnetic field strength and magnetic susceptibility of the materials within the field. Compounds that have paramagnetic, diamagnetic, or ferromagnetic properties interact with and alter the local magnetic field, resulting in heterogeneity of spins of local protons; as a result, the protons precess at different rates and cause signal loss, called "susceptibility artifact," that is most prominent in T2*-weighted images (Haacke et al. 2004, 2009; Tong et al. 2008). Paramagnetic compounds include deoxyhemoglobin, ferritin, and hemosiderin, while diamagnetic compounds include bone minerals and dystrophic calcifications (Schweser et al. 2010).

Compounds with susceptibility artifact will manifest on MR imaging as hypointense signal. On the routine processed images, there is no differentiation between compounds—all our hypointense. Phase imaging, which is part of the SWI data set in certain vendors, permits this differentiation, namely, blood products versus calcium, a not uncommon question in clinical imaging, especially in the absence of CT imaging. Blood products are hypointense on the phase images since deoxygenated blood is paramagnetic relative to

surrounding tissue, while calcium is hyperintense since it is diamagnetic relative to surrounding tissue (Haacke et al. 2009).

## 13.7.3 Applications

The main application of SWI for tumor imaging is to detect hemorrhage, vascularity, and calcification characteristics that may reflect tumor grade. Calcification can be seen in lower grade tumors such as oligodendroglioma, while hemorrhage and marked vascularity may be seen in higher grade tumors, related to neoangiogenesis.

Evaluating the presence of hemorrhage has implications in management and treatment. Preoperatively, SWI can help plan the surgical approach for biopsy or resection by assessing the site of intra-tumoral hemorrhage. With regard to posttreatment analysis, hemorrhage may be seen in postoperative setting of surgery or radiosurgery. In patients that are being treated with anti-angiogenic therapy, the presence of hemorrhage on SWI may have implications in treatment course (Grabner et al. 2012). While a significant amount of hemorrhage may halt therapy, increasing SWI hypointensity within a tumor may in fact signify a better prognosis by implying less active tumor

(Lupo et al. 2013). Further research is needed to validate results.

SWI imaging is also sensitive for identifying vasculopathy resulting from radiation therapy; these lesions, usually referred to as "telangiectasias and cavernous malformations," are particularly common in children after cranial irradiation (Koike et al. 2004; Larson et al. 1998).

## 13.8   Improving Image Sensitivity to Analyze Small Tumors

Subtle or small neoplasms of the cortex (ganglioglioma, DNET), internal auditory canal (schwannoma in neurofibromatosis), and spinal cord (astrocytoma, ependymoma) can be missed on traditional MR sequences. There are primarily two methods to increase sensitivity to detect and characterize these neoplasms when they are small: higher resolution images obtained with a high-field-strength magnet (>4 T) or imaging with a routine strength magnet and using special coils and software (Moyher et al. 1997). In the past, use of phased array surface coils and image intensity correction algorithms increased the signal-to-noise ratio for superficial lesions beyond traditional imaging sequences. Newer multichannel coils, using parallel imaging, are now commercially available as an alternative to surface coils and provide similar sensitivity.

Magnetization transfer is a technique that allows imaging of molecules that interact with macromolecules in the brain (predominantly the components of myelin) separately from free, unbound water molecules. The major application of magnetization transfer imaging for brain tumors is to increase lesion conspicuity; by reducing the hyperintensity of white matter on T1-weighted images, enhancement becomes more conspicuous.

### Conclusions

Neuroradiologic evaluation of tumors has grown to include many more techniques than anatomic imaging. Metabolic assessment, assessment of perfusion, and assessment of the function of surrounding brain can now be performed along with anatomic imaging in a single visit to the MR suite. These techniques provide useful tools to assess the character of pediatric brain tumors and their responses to therapy.

## References

Alberstone CD, Skirboll SL, Benzel EC et al (2000) Magnetic source imaging and brain surgery: presurgical and intraoperative planning in 26 patients. J Neurosurg 92:79–90

Aronen HJ, Gazit IE, Louis DN et al (1994) Cerebral blood volume maps of gliomas: comparison with tumor grade and histologic findings. Radiology 191:41–51

Ball WS Jr, Holland SK (2001) Perfusion imaging in the pediatric patient. Magn Reson Imaging Clin N Am 9:207–230, ix

Barker PB, Glickson JD, Bryan RN (1993) In vivo magnetic resonance spectroscopy of human brain tumors. Top Magn Reson Imaging 5:32–45

Barker FG 2nd, Chang SM, Valk PE, Pounds TR, Prados MD (1997) 18-Fluorodeoxyglucose uptake and survival of patients with suspected recurrent malignant glioma. Cancer 79:115–126

Beisteiner R, Gomiscek G, Erdler M, Teichtmeister C, Moser E, Deecke L (1995) Comparing localization of conventional functional magnetic resonance imaging and magnetoencephalography. Eur J Neurosci 7:1121–1124

Belanger M, Allaman I, Magistretti PJ (2011) Brain energy metabolism: focus on astrocyte-neuron metabolic cooperation. Cell Metab 14:724–738

Birken DL, Oldendorf WH (1989) N-acetyl-L-aspartic acid: a literature review of a compound prominent in 1H-NMR spectroscopic studies of brain. Neurosci Biobehav Rev 13:23–31

Black KL, Emerick T, Hoh C, Hawkins RA, Mazziotta J, Becker DP (1994) Thallium-201 SPECT and positron emission tomography equal predictors of glioma grade and recurrence. Neurol Res 16:93–96

Boxerman JL, Bandettini PA, Kwong KK et al (1995) The intravascular contribution to fMRI signal change: Monte Carlo modeling and diffusion-weighted studies in vivo. Magn Reson Med 34:4–10

Bradbury MS, Hambardzumyan D, Zanzonico PB et al (2008) Dynamic small-animal PET imaging of tumor proliferation with 3′-deoxy-3′-18F-fluorothymidine in a genetically engineered mouse model of high-grade gliomas. J Nucl Med 49:422–429

Breier JI, Simos PG, Zouridakis G et al (1999) Language dominance determined by magnetic source imaging: a comparison with the Wada procedure. Neurology 53:938–945

Bruggers CS, Moore K (2014) Magnetic resonance imaging spectroscopy in pediatric atypical teratoid rhabdoid tumors of the brain. J Pediatr Hematol Oncol 36:e341–e345

Brunelle F (2000) Noninvasive diagnosis of brain tumours in children. Childs Nerv Syst 16:731–734

Butzen J, Prost R, Chetty V et al (2000) Discrimination between neoplastic and nonneoplastic brain lesions by use of proton MR spectroscopy: the limits of accuracy with a logistic regression model. AJNR Am J Neuroradiol 21:1213–1219

Cappabianca P, Spaziante R, Caputi F et al (1991) Accuracy of the analysis of multiple small fragments of glial tumors obtained by stereotactic biopsy. Acta Cytol 35:505–511

Cedzich C, Taniguchi M, Schafer S, Schramm J (1996) Somatosensory evoked potential phase reversal and direct motor cortex stimulation during surgery in and around the central region. Neurosurgery 38:962–970

Cha S (2006) Update on brain tumor imaging: from anatomy to physiology. AJNR Am J Neuroradiol 27:475–487

Cha S, Lu S, Johnson G, Knopp EA (2000a) Dynamic susceptibility contrast MR imaging: correlation of signal intensity changes with cerebral blood volume measurements. J Magn Reson Imaging 11:114–119

Cha S, Knopp EA, Johnson G et al (2000b) Dynamic contrast-enhanced T2-weighted MR imaging of recurrent malignant gliomas treated with thalidomide and carboplatin. AJNR Am J Neuroradiol 21:881–890

Cha S, Knopp EA, Johnson G, Wetzel SG, Litt AW, Zagzag D (2002) Intracranial mass lesions: dynamic contrast-enhanced susceptibility-weighted echo-planar perfusion MR imaging. Radiology 223:11–29

Chan YL, Leung SF, King AD, Choi PH, Metreweli C (1999) Late radiation injury to the temporal lobes: morphologic evaluation at MR imaging. Radiology 213:800–807

Chandrasoma PT, Smith MM, Apuzzo ML (1989) Stereotactic biopsy in the diagnosis of brain masses: comparison of results of biopsy and resected surgical specimen. Neurosurgery 24:160–165

Chang KH, Song IC, Kim SH et al (1998) In vivo single-voxel proton MR spectroscopy in intracranial cystic masses. AJNR Am J Neuroradiol 19:401–405

Chawla A, Emmanuel JV, Seow WT, Lou J, Teo HE, Lim CC (2007) Paediatric PNET: pre-surgical MRI features. Clin Radiol 62:43–52

Chen W, Silverman DH (2008) Advances in evaluation of primary brain tumors. Semin Nucl Med 38:240–250

Chen HJ, Panigrahy A, Dhall G, Finlay JL, Nelson MD Jr, Bluml S (2010) Apparent diffusion and fractional anisotropy of diffuse intrinsic brain stem gliomas. AJNR Am J Neuroradiol 31:1879–1885

Choi JY, Kim SE, Shin HJ, Kim BT, Kim JH (2000) Brain tumor imaging with 99mTc-tetrofosmin: comparison with 201Tl, 99mTc-MIBI, and 18F-fluorodeoxyglucose. J Neurooncol 46:63–70

Choi C, Ganji SK, DeBerardinis RJ et al (2012) 2-hydroxyglutarate detection by magnetic resonance spectroscopy in IDH-mutated patients with gliomas. Nat Med 18:624–629

Dadparvar S, Hussain R, Koffler SP, Gillan MM, Bartolic EI, Miyamoto C (2000) The role of Tc-99m HMPAO functional brain imaging in detection of cerebral radionecrosis. Cancer J 6:381–387

De Witte O, Lefranc F, Levivier M, Salmon I, Brotchi J, Goldman S (2000) FDG-PET as a prognostic factor in high-grade astrocytoma. J Neurooncol 49:157–163

Dezortova M, Hajek M, Cap F, Babis M, Tichy M, Vymazal J (1999) Comparison of MR spectroscopy and MR imaging with contrast agent in children with cerebral astrocytomas. Childs Nerv Syst 15:408–412

Di Chiro G, Oldfield E, Wright DC et al (1988) Cerebral necrosis after radiotherapy and/or intraarterial chemotherapy for brain tumors: PET and neuropathologic studies. AJR Am J Roentgenol 150:189–197

Dillon WP, Roberts T (1999) The limitations of functional MR imaging: a caveat. AJNR Am J Neuroradiol 20:536

Disbrow E, Roberts TP, Slutsky D, Krubitzer L (1999) The use of fMRI for determining the topographic organization of cortical fields in human and nonhuman primates. Brain Res 829:167–173

Dowling C, Bollen AW, Noworolski SM et al (2001) Preoperative proton MR spectroscopic imaging of brain tumors: correlation with histopathologic analysis of resection specimens. AJNR Am J Neuroradiol 22:604–612

Dunkl V, Cleff C, Stoffels G et al (2015) The usefulness of dynamic O-(2-18F-Fluoroethyl)-l-tyrosine PET in the clinical evaluation of brain tumors in children and adolescents. J Nucl Med 56:88–92

Essig M, Shiroishi MS, Nguyen TB et al (2013) Perfusion MRI: the five most frequently asked technical questions. AJR Am J Roentgenol 200:24–34

Field AS, Yen YF, Burdette JH, Elster AD (2000) False cerebral activation on BOLD functional MR images: study of low-amplitude motion weakly correlated to stimulus. AJNR Am J Neuroradiol 21:1388–1396

Filippi M, Cercignani M, Inglese M, Horsfield MA, Comi G (2001) Diffusion tensor magnetic resonance imaging in multiple sclerosis. Neurology 56:304–311

Ganslandt O, Fahlbusch R, Nimsky C et al (1999) Functional neuronavigation with magnetoencephalography: outcome in 50 patients with lesions around the motor cortex. Neurosurg Focus 6, e3

Gauvain KM, McKinstry RC, Mukherjee P et al (2001) Evaluating pediatric brain tumor cellularity with diffusion-tensor imaging. AJR Am J Roentgenol 177:449–454

Gerlowski LE, Jain RK (1986) Microvascular permeability of normal and neoplastic tissues. Microvasc Res 31:288–305

Giannini C, Scheithauer BW (1997) Classification and grading of low-grade astrocytic tumors in children. Brain Pathol 7:785–798

Girard N, Wang ZJ, Erbetta A et al (1998) Prognostic value of proton MR spectroscopy of cerebral hemisphere tumors in children. Neuroradiology 40:121–125

Go KG, Keuter EJ, Kamman RL et al (1994) Contribution of magnetic resonance spectroscopic imaging and

L-[1-11C]tyrosine positron emission tomography to localization of cerebral gliomas for biopsy. Neurosurgery 34:994–1002, discussion 1002

Golay X, Petersen ET (2006) Arterial spin labeling: benefits and pitfalls of high magnetic field. Neuroimaging Clin N Am 16:259–268, x

Grabner G, Nobauer I, Elandt K et al (2012) Longitudinal brain imaging of five malignant glioma patients treated with bevacizumab using susceptibility-weighted magnetic resonance imaging at 7 T. Magn Reson Imaging 30:139–147

Grand S, Passaro G, Ziegler A et al (1999) Necrotic tumor versus brain abscess: importance of amino acids detected at 1H MR spectroscopy – initial results. Radiology 213:785–793

Greenwood J (1991) Mechanisms of blood-brain barrier breakdown. Neuroradiology 33:95–100

Gupta RK, Vatsal DK, Husain N et al (2001) Differentiation of tuberculous from pyogenic brain abscesses with in vivo proton MR spectroscopy and magnetization transfer MR imaging. AJNR Am J Neuroradiol 22:1503–1509

Haacke EM, Xu Y, Cheng YC, Reichenbach JR (2004) Susceptibility weighted imaging (SWI). Magn Reson Med 52:612–618

Haacke EM, Mittal S, Wu Z, Neelavalli J, Cheng YC (2009) Susceptibility-weighted imaging: technical aspects and clinical applications, part 1. AJNR Am J Neuroradiol 30:19–30

Hatakeyama T, Kawai N, Nishiyama Y et al (2008) (11)C-methionine (MET) and (18)F-fluorothymidine (FLT) PET in patients with newly diagnosed glioma. Eur J Nucl Med Mol Imaging 35:2009–2017

Hayes LL, Jones RA, Palasis S, Aguilera D, Porter DA (2012) Drop metastases to the pediatric spine revealed with diffusion-weighted MR imaging. Pediatr Radiol 42:1009–1013

Holodny AI, Schulder M, Liu WC, Maldjian JA, Kalnin AJ (1999) Decreased BOLD functional MR activation of the motor and sensory cortices adjacent to a glioblastoma multiforme: implications for image-guided neurosurgery. AJNR Am J Neuroradiol 20:609–612

Horska A, Ulug AM, Melhem ER et al (2001) Proton magnetic resonance spectroscopy of choroid plexus tumors in children. J Magn Reson Imaging 14:78–82

Hunter JV, Wang ZJ (2001) MR spectroscopy in pediatric neuroradiology. Magn Reson Imaging Clin N Am 9:165–189, ix

Inglis BA, Neubauer D, Yang L, Plant D, Mareci TH, Muir D (1999) Diffusion tensor MR imaging and comparative histology of glioma engrafted in the rat spinal cord. AJNR Am J Neuroradiol 20:713–716

Jaremko JL, Jans LB, Coleman LT, Ditchfield MR (2010) Value and limitations of diffusion-weighted imaging in grading and diagnosis of pediatric posterior fossa tumors. AJNR Am J Neuroradiol 31:1613–1616

Joyce P, Bentson J, Takahashi M, Winter J, Wilson G, Byrd S (1978) The accuracy of predicting histologic grades of supratentorial astrocytomas on the basis of computerized tomography and cerebral angiography. Neuroradiology 16:346–348

Kamada K, Houkin K, Abe H, Sawamura Y, Kashiwaba T (1997) Differentiation of cerebral radiation necrosis from tumor recurrence by proton magnetic resonance spectroscopy. Neurol Med Chir (Tokyo) 37:250–256

Kaplan WD, Takvorian T, Morris JH, Rumbaugh CL, Connolly BT, Atkins HL (1987) Thallium-201 brain tumor imaging: a comparative study with pathologic correlation. J Nucl Med 28:47–52

Kaplan AM, Bandy DJ, Manwaring KH et al (1999) Functional brain mapping using positron emission tomography scanning in preoperative neurosurgical planning for pediatric brain tumors. J Neurosurg 91:797–803

Keene DL, Hsu E, Ventureyra E (1999) Brain tumors in childhood and adolescence. Pediatr Neurol 20:198–203

Keles GE, Chang EF, Lamborn KR et al (2006) Volumetric extent of resection and residual contrast enhancement on initial surgery as predictors of outcome in adult patients with hemispheric anaplastic astrocytoma. J Neurosurg 105:34–40

Kim EE, Chung SK, Haynie TP et al (1992) Differentiation of residual or recurrent tumors from post-treatment changes with F-18 FDG PET. Radiographics 12:269–279

Kim SH, Chang KH, Song IC et al (1997) Brain abscess and brain tumor: discrimination with in vivo H-1 MR spectroscopy. Radiology 204:239–245

Kimura T, Sako K, Gotoh T, Tanaka K, Tanaka T (2001) In vivo single-voxel proton MR spectroscopy in brain lesions with ring-like enhancement. NMR Biomed 14:339–349

Kincaid PK, El-Saden SM, Park SH, Goy BW (1998) Cerebral gangliogliomas: preoperative grading using FDG-PET and 201Tl-SPECT. AJNR Am J Neuroradiol 19:801–806

Kinoshita Y, Yokota A (1997) Absolute concentrations of metabolites in human brain tumors using in vitro proton magnetic resonance spectroscopy. NMR Biomed 10:2–12

Knopp EA, Cha S, Johnson G et al (1999) Glial neoplasms: dynamic contrast-enhanced T2*-weighted MR imaging. Radiology 211:791–798

Koike S, Aida N, Hata M, Fujita K, Ozawa Y, Inoue T (2004) Asymptomatic radiation-induced telangiectasia in children after cranial irradiation: frequency, latency, and dose relation. Radiology 230:93–99

Koral K, Zhang S, Gargan L et al (2013) Diffusion MRI improves the accuracy of preoperative diagnosis of common pediatric cerebellar tumors among reviewers with different experience levels. AJNR Am J Neuroradiol 34:2360–2365

Krishnamoorthy T, Radhakrishnan VV, Thomas B, Jeyadevan ER, Menon G, Nair S (2007) Alanine peak in central neurocytomas on proton MR spectroscopy. Neuroradiology 49:551–554

Krouwer HG, Kim TA, Rand SD et al (1998) Single-voxel proton MR spectroscopy of nonneoplastic brain

lesions suggestive of a neoplasm. AJNR Am J Neuroradiol 19:1695–1703

Kugel H, Heindel W, Ernestus RI, Bunke J, du Mesnil R, Friedmann G (1992) Human brain tumors: spectral patterns detected with localized H-1 MR spectroscopy. Radiology 183:701–709

Lam WW, Poon WS, Metreweli C (2002) Diffusion MR imaging in glioma: does it have any role in the pre-operation determination of grading of glioma? Clin Radiol 57:219–225

Larson JJ, Ball WS, Bove KE, Crone KR, Tew JM Jr (1998) Formation of intracerebral cavernous malformations after radiation treatment for central nervous system neoplasia in children. J Neurosurg 88:51–56

Law M, Cha S, Knopp EA, Johnson G, Arnett J, Litt AW (2002) High-grade gliomas and solitary metastases: differentiation by using perfusion and proton spectroscopic MR imaging. Radiology 222:715–721

Lazareff JA, Gupta RK, Alger J (1999) Variation of post-treatment H-MRSI choline intensity in pediatric gliomas. J Neurooncol 41:291–298

Lehnhardt FG, Rohn G, Ernestus RI, Grune M, Hoehn M (2001) 1H- and (31)P-MR spectroscopy of primary and recurrent human brain tumors in vitro: malignancy-characteristic profiles of water soluble and lipophilic spectral components. NMR Biomed 14:307–317

Lev MH, Grant PE (2000) MEG versus BOLD MR imaging: functional imaging, the next generation? AJNR Am J Neuroradiol 21:1369–1370

Lin A, Bluml S, Mamelak AN (1999) Efficacy of proton magnetic resonance spectroscopy in clinical decision making for patients with suspected malignant brain tumors. J Neurooncol 45:69–81

Lorberboym M, Mandell LR, Mosesson RE et al (1997) The role of thallium-201 uptake and retention in intracranial tumors after radiotherapy. J Nucl Med 38:223–226

Ludemann L, Hamm B, Zimmer C (2000) Pharmacokinetic analysis of glioma compartments with dynamic Gd-DTPA-enhanced magnetic resonance imaging. Magn Reson Imaging 18:1201–1214

Lupo JM, Essock-Burns E, Molinaro AM et al (2013) Using susceptibility-weighted imaging to determine response to combined anti-angiogenic, cytotoxic, and radiation therapy in patients with glioblastoma multiforme. Neuro Oncol 15:480–489

Maeda M, Itoh S, Kimura H et al (1993) Tumor vascularity in the brain: evaluation with dynamic susceptibility-contrast MR imaging. Radiology 189:233–238

Maria BL, Drane WE, Quisling RG et al (1994) Value of thallium-201 SPECT imaging in childhood brain tumors. Pediatr Neurosurg 20:11–18

Maria BL, Drane WB, Quisling RJ, Hoang KB (1997) Correlation between gadolinium-diethylenetriaminepentaacetic acid contrast enhancement and thallium-201 chloride uptake in pediatric brainstem glioma. J Child Neurol 12:341–348

Maria BL, Drane WE, Mastin ST, Jimenez LA (1998) Comparative value of thallium and glucose SPECT

imaging in childhood brain tumors. Pediatr Neurol 19:351–357

Martin E, Marcar VL (2001) Functional MR imaging in pediatrics. Magn Reson Imaging Clin N Am 9:231–246, ix-x

Martin AJ, Liu H, Hall WA, Truwit CL (2001) Preliminary assessment of turbo spectroscopic imaging for targeting in brain biopsy. AJNR Am J Neuroradiol 22:959–968

Massager N, David P, Goldman S et al (2000) Combined magnetic resonance imaging- and positron emission tomography-guided stereotactic biopsy in brainstem mass lesions: diagnostic yield in a series of 30 patients. J Neurosurg 93:951–957

McKnight TR, Noworolski SM, Vigneron DB, Nelson SJ (2001) An automated technique for the quantitative assessment of 3D-MRSI data from patients with glioma. J Magn Reson Imaging 13:167–177

Melhem ER, Itoh R, Jones L, Barker PB (2000) Diffusion tensor MR imaging of the brain: effect of diffusion weighting on trace and anisotropy measurements. AJNR Am J Neuroradiol 21:1813–1820

Mettler FA Jr, Huda W, Yoshizumi TT, Mahesh M (2008) Effective doses in radiology and diagnostic nuclear medicine: a catalog. Radiology 248:254–263

Mitchell DG (1999) MRI Principles. WB Saunders, Philadelphia

Moreno-Torres A, Martinez-Perez I, Baquero M et al (2004) Taurine detection by proton magnetic resonance spectroscopy in medulloblastoma: contribution to noninvasive differential diagnosis with cerebellar astrocytoma. Neurosurgery 55:824–829, discussion 829

Moyher SE, Wald LL, Nelson SJ et al (1997) High resolution T2-weighted imaging of the human brain using surface coils and an analytical reception profile correction. J Magn Reson Imaging 7:512–517

Muzi M, Spence AM, O'Sullivan F et al (2006) Kinetic analysis of 3′-deoxy-3′-18F-fluorothymidine in patients with gliomas. J Nucl Med 47:1612–1621

Negendank WG, Sauter R, Brown TR et al (1996) Proton magnetic resonance spectroscopy in patients with glial tumors: a multicenter study. J Neurosurg 84:449–458

Nelson SJ, Nalbandian AB, Proctor E, Vigneron DB (1994) Registration of images from sequential MR studies of the brain. J Magn Reson Imaging 4:877–883

Nelson SJ, Huhn S, Vigneron DB et al (1997a) Volume MRI and MRSI techniques for the quantitation of treatment response in brain tumors: presentation of a detailed case study. J Magn Reson Imaging 7:1146–1152

Nelson SJ, Vigneron DB, Star-Lack J, Kurhanewicz J (1997b) High spatial resolution and speed in MRSI. NMR Biomed 10:411–422

Nelson SJ, Vigneron DB, Dillon WP (1999) Serial evaluation of patients with brain tumors using volume MRI and 3D 1H MRSI. NMR Biomed 12:123–138

Norfray JF, Tomita T, Byrd SE, Ross BD, Berger PA, Miller RS (1999) Clinical impact of MR spectroscopy

when MR imaging is indeterminate for pediatric brain tumors. AJR Am J Roentgenol 173:119–125

Ogawa T, Kanno I, Shishido F et al (1991) Clinical value of PET with 18F-fluorodeoxyglucose and L-methyl-11C-methionine for diagnosis of recurrent brain tumor and radiation injury. Acta Radiol 32:197–202

Otsubo H, Snead OC 3rd (2001) Magnetoencephalography and magnetic source imaging in children. J Child Neurol 16:227–235

Ott D, Hennig J, Ernst T (1993) Human brain tumors: assessment with in vivo proton MR spectroscopy. Radiology 186:745–752

O'Tuama LA, Poussaint TY, Anthony DC, Treves ST (1998) Childhood brain tumor: neuroimaging correlated with disease outcome. Pediatr Neurol 19:259–262

Papanicolaou AC, Simos PG, Breier JI et al (2001) Brain plasticity for sensory and linguistic functions: a functional imaging study using magnetoencephalography with children and young adults. J Child Neurol 16:241–252

Peters AM (1998) Fundamentals of tracer kinetics for radiologists. Br J Radiol 71:1116–1129

Pierpaoli C, Jezzard P, Basser PJ, Barnett A, Di Chiro G (1996) Diffusion tensor MR imaging of the human brain. Radiology 201:637–648

Pirotte B, Acerbi F, Lubansu A, Goldman S, Brotchi J, Levivier M (2007) PET imaging in the surgical management of pediatric brain tumors. Childs Nerv Syst 23:739–751

Plate KH, Mennel HD (1995) Vascular morphology and angiogenesis in glial tumors. Exp Toxicol Pathol 47:89–94

Poptani H, Gupta RK, Roy R, Pandey R, Jain VK, Chhabra DK (1995) Characterization of intracranial mass lesions with in vivo proton MR spectroscopy. AJNR Am J Neuroradiol 16:1593–1603

Poupon C, Clark CA, Frouin V et al (2000) Regularization of diffusion-based direction maps for the tracking of brain white matter fascicles. Neuroimage 12:184–195

Poussaint TY, Siffert J, Barnes PD et al (1995) Hemorrhagic vasculopathy after treatment of central nervous system neoplasia in childhood: diagnosis and follow-up. AJNR Am J Neuroradiol 16:693–699

Provenzale JM, Arata MA, Turkington TG, McLendon RE, Coleman RE (1999) Gangliogliomas: characterization by registered positron emission tomography-MR images. AJR Am J Roentgenol 172:1103–1107

Pujol J, Conesa G, Deus J, Lopez-Obarrio L, Isamat F, Capdevila A (1998) Clinical application of functional magnetic resonance imaging in presurgical identification of the central sulcus. J Neurosurg 88:863–869

Puttick S, Bell C, Dowson N, Rose S, Fay M (2014) PET, MRI, and simultaneous PET/MRI in the development of diagnostic and therapeutic strategies for glioma. Drug Discov Today

Ricci PE, Karis JP, Heiserman JE, Fram EK, Bice AN, Drayer BP (1998) Differentiating recurrent tumor from radiation necrosis: time for re-evaluation of positron emission tomography? AJNR Am J Neuroradiol 19:407–413

Roberts TP, Rowley HA (1997) Mapping of the sensorimotor cortex: functional MR and magnetic source imaging. AJNR Am J Neuroradiol 18:871–880

Roberts HC, Roberts TP, Brasch RC, Dillon WP (2000a) Quantitative measurement of microvascular permeability in human brain tumors achieved using dynamic contrast-enhanced MR imaging: correlation with histologic grade. AJNR Am J Neuroradiol 21:891–899

Roberts TP, Disbrow EA, Roberts HC, Rowley HA (2000b) Quantification and reproducibility of tracking cortical extent of activation by use of functional MR imaging and magnetoencephalography. AJNR Am J Neuroradiol 21:1377–1387

Rosen BR, Belliveau JW, Vevea JM, Brady TJ (1990) Perfusion imaging with NMR contrast agents. Magn Reson Med 14:249–265

Rosen BR, Belliveau JW, Aronen HJ et al (1991) Susceptibility contrast imaging of cerebral blood volume: human experience. Magn Reson Med 22:293–299, discussion 300-293

Salibi N, Brown MA (1998) Clinical MR spectroscopy (first principles). Wiley-Liss, New York

Saritas EU, Cunningham CH, Lee JH, Han ET, Nishimura DG (2008) DWI of the spinal cord with reduced FOV single-shot EPI. Magn Reson Med 60:468–473

Schweser F, Deistung A, Lehr BW, Reichenbach JR (2010) Differentiation between diamagnetic and paramagnetic cerebral lesions based on magnetic susceptibility mapping. Med Phys 37:5165–5178

Seymour ZA, Panigrahy A, Finlay JL, Nelson MD Jr, Bluml S (2008) Citrate in pediatric CNS tumors? AJNR Am J Neuroradiol 29:1006–1011

Shimizu H, Kumabe T, Tominaga T et al (1996) Noninvasive evaluation of malignancy of brain tumors with proton MR spectroscopy. AJNR Am J Neuroradiol 17:737–747

Shino A, Nakasu S, Matsuda M, Handa J, Morikawa S, Inubushi T (1999) Noninvasive evaluation of the malignant potential of intracranial meningiomas performed using proton magnetic resonance spectroscopy. J Neurosurg 91:928–934

Shinoura N, Nishijima M, Hara T et al (1997) Brain tumors: detection with C-11 choline PET. Radiology 202:497–503

Shtern F (1992) Clinical experimentation in magnetic resonance spectroscopy: a perspective from the National Cancer Institute. NMR Biomed 5:325–328

Shukla-Dave A, Gupta RK, Roy R et al (2001) Prospective evaluation of in vivo proton MR spectroscopy in differentiation of similar appearing intracranial cystic lesions. Magn Reson Imaging 19:103–110

Siegal T, Rubinstein R, Tzuk-Shina T, Gomori JM (1997) Utility of relative cerebral blood volume mapping derived from perfusion magnetic resonance imaging in the routine follow up of brain tumors. J Neurosurg 86:22–27

Sijens PE, Vecht CJ, Levendag PC, van Dijk P, Oudkerk M (1995) Hydrogen magnetic resonance spectroscopy

follow-up after radiation therapy of human brain cancer. Unexpected inverse correlation between the changes in tumor choline level and post-gadolinium magnetic resonance imaging contrast. Invest Radiol 30:738–744

Simos PG, Papanicolaou AC, Breier JI et al (1999) Localization of language-specific cortex by using magnetic source imaging and electrical stimulation mapping. J Neurosurg 91:787–796

Smith JS, Cha S, Mayo MC et al (2005) Serial diffusion-weighted magnetic resonance imaging in cases of glioma: distinguishing tumor recurrence from postresection injury. J Neurosurg 103:428–438

Smith JS, Chang EF, Lamborn KR et al (2008) Role of extent of resection in the long-term outcome of low-grade hemispheric gliomas. J Clin Oncol 26:1338–1345

Stadnik TW, Chaskis C, Michotte A et al (2001) Diffusion-weighted MR imaging of intracerebral masses: comparison with conventional MR imaging and histologic findings. AJNR Am J Neuroradiol 22:969–976

Stippich C, Freitag P, Kassubek J et al (1998) Motor, somatosensory and auditory cortex localization by fMRI and MEG. Neuroreport 9:1953–1957

Strong JA, Hatten HP Jr, Brown MT et al (1993) Pilocytic astrocytoma: correlation between the initial imaging features and clinical aggressiveness. AJR Am J Roentgenol 161:369–372

Sugahara T, Korogi Y, Kochi M et al (1998) Correlation of MR imaging-determined cerebral blood volume maps with histologic and angiographic determination of vascularity of gliomas. AJR Am J Roentgenol 171:1479–1486

Sugahara T, Korogi Y, Shigematsu Y et al (1999) Value of dynamic susceptibility contrast magnetic resonance imaging in the evaluation of intracranial tumors. Top Magn Reson Imaging 10:114–124

Sugahara T, Korogi Y, Tomiguchi S et al (2000) Posttherapeutic intraaxial brain tumor: the value of perfusion-sensitive contrast-enhanced MR imaging for differentiating tumor recurrence from nonneoplastic contrast-enhancing tissue. AJNR Am J Neuroradiol 21:901–909

Sugahara T, Korogi Y, Kochi M, Ushio Y, Takahashi M (2001) Perfusion-sensitive MR imaging of gliomas: comparison between gradient-echo and spin-echo echo-planar imaging techniques. AJNR Am J Neuroradiol 22:1306–1315

Sutton LN, Wang Z, Gusnard D et al (1992) Proton magnetic resonance spectroscopy of pediatric brain tumors. Neurosurgery 31:195–202

Suzuki A, Yasui N (1992) Intraoperative localization of the central sulcus by cortical somatosensory evoked potentials in brain tumor. Case report. J Neurosurg 76:867–870

Szigety SK, Allen PS, Huyser-Wierenga D, Urtasun RC (1993) The effect of radiation on normal human CNS as detected by NMR spectroscopy. Int J Radiat Oncol Biol Phys 25:695–701

Szymanski MD, Perry DW, Gage NM et al (2001) Magnetic source imaging of late evoked field responses to vowels: toward an assessment of hemispheric dominance for language. J Neurosurg 94:445–453

Tanner SF, Ramenghi LA, Ridgway JP et al (2000) Quantitative comparison of intrabrain diffusion in adults and preterm and term neonates and infants. AJR Am J Roentgenol 174:1643–1649

Taylor JS, Langston JW, Reddick WE et al (1996) Clinical value of proton magnetic resonance spectroscopy for differentiating recurrent or residual brain tumor from delayed cerebral necrosis. Int J Radiat Oncol Biol Phys 36:1251–1261

Tomoi M, Kimura H, Yoshida M et al (1997) Alterations of lactate (+lipid) concentration in brain tumors with in vivo hydrogen magnetic resonance spectroscopy during radiotherapy. Invest Radiol 32:288–296

Tong KA, Ashwal S, Obenaus A, Nickerson JP, Kido D, Haacke EM (2008) Susceptibility-weighted MR imaging: a review of clinical applications in children. AJNR Am J Neuroradiol 29:9–17

Tzika AA, Vigneron DB, Dunn RS, Nelson SJ, Ball WS Jr (1996) Intracranial tumors in children: small single-voxel proton MR spectroscopy using short- and long-echo sequences. Neuroradiology 38:254–263

Tzika AA, Vajapeyam S, Barnes PD (1997) Multivoxel proton MR spectroscopy and hemodynamic MR imaging of childhood brain tumors: preliminary observations. AJNR Am J Neuroradiol 18:203–218

Tzika AA, Zurakowski D, Poussaint TY et al (2001) Proton magnetic spectroscopic imaging of the child's brain: the response of tumors to treatment. Neuroradiology 43:169–177

Tzika AA, Zarifi MK, Goumnerova L et al (2002) Neuroimaging in pediatric brain tumors: Gd-DTPA-enhanced, hemodynamic, and diffusion MR imaging compared with MR spectroscopic imaging. AJNR Am J Neuroradiol 23:322–333

Ullrich R, Backes H, Li H et al (2008) Glioma proliferation as assessed by 3′-fluoro-3′-deoxy-L-thymidine positron emission tomography in patients with newly diagnosed high-grade glioma. Clin Cancer Res 14:2049–2055

Urenjak J, Williams SR, Gadian DG, Noble M (1993) Proton nuclear magnetic resonance spectroscopy unambiguously identifies different neural cell types. J Neurosci 13:981–989

Usenius T, Usenius JP, Tenhunen M et al (1995) Radiation-induced changes in human brain metabolites as studied by 1H nuclear magnetic resonance spectroscopy in vivo. Int J Radiat Oncol Biol Phys 33:719–724

Valk PE, Dillon WP (1991) Radiation injury of the brain. AJNR Am J Neuroradiol 12:45–62

Valk PE, Budinger TF, Levin VA, Silver P, Gutin PH, Doyle WK (1988) PET of malignant cerebral tumors after interstitial brachytherapy. Demonstration of metabolic activity and correlation with clinical outcome. J Neurosurg 69:830–838

van Gelderen P, de Zwart JA, Duyn JH (2008) Pittfalls of MRI measurement of white matter perfusion based on arterial spin labeling. Magn Reson Med 59:788–795

Venkatesh SK, Gupta RK, Pal L, Husain N, Husain M (2001) Spectroscopic increase in choline signal is a nonspecific marker for differentiation of infective/inflammatory from neoplastic lesions of the brain. J Magn Reson Imaging 14:8–15

Vezina LG (1997) Diagnostic imaging in neuro-oncology. Pediatr Clin N Am 44:701–719

Vigneron D, Bollen A, McDermott M et al (2001) Three-dimensional magnetic resonance spectroscopic imaging of histologically confirmed brain tumors. Magn Reson Imaging 19:89–101

Waldrop SM, Davis PC, Padgett CA, Shapiro MB, Morris R (1998) Treatment of brain tumors in children is associated with abnormal MR spectroscopic ratios in brain tissue remote from the tumor site. AJNR Am J Neuroradiol 19:963–970

Wang Z, Sutton LN, Cnaan A et al (1995) Proton MR spectroscopy of pediatric cerebellar tumors. AJNR Am J Neuroradiol 16:1821–1833

Wang Z, Zimmerman RA, Sauter R (1996a) Proton MR spectroscopy of the brain: clinically useful information obtained in assessing CNS diseases in children. AJR Am J Roentgenol 167:191–199

Wang GJ, Volkow ND, Lau YH et al (1996b) Glucose metabolic changes in nontumoral brain tissue of patients with brain tumor following radiotherapy: a preliminary study. J Comput Assist Tomogr 20:709–714

Weisskoff RM, Zuo CS, Boxerman JL, Rosen BR (1994) Microscopic susceptibility variation and transverse relaxation: theory and experiment. Magn Reson Med 31:601–610

Wheless JW, Willmore LJ, Breier JI et al (1999) A comparison of magnetoencephalography, MRI, and V-EEG in patients evaluated for epilepsy surgery. Epilepsia 40:931–941

Wilken B, Dechent P, Herms J et al (2000) Quantitative proton magnetic resonance spectroscopy of focal brain lesions. Pediatr Neurol 23:22–31

Wilson M, Gill SK, MacPherson L, English M, Arvanitis TN, Peet AC (2014) Noninvasive detection of glutamate predicts survival in pediatric medulloblastoma. Clin Cancer Res 20:4532–4539

Yeom KW, Lober RM, Andre JB et al (2013) Prognostic role for diffusion-weighted imaging of pediatric optic pathway glioma. J Neurooncol 113:479–483

Yeom KW, Mitchell LA, Lober RM et al (2014) Arterial spin-labeled perfusion of pediatric brain tumors. AJNR Am J Neuroradiol 35:395–401

Yeung DK, Chan Y, Leung S, Poon PM, Pang C (2001) Detection of an intense resonance at 2.4 ppm in 1H MR spectra of patients with severe late-delayed, radiation-induced brain injuries. Magn Reson Med 45:994–1000

Yousem DM, Lenkinski RE, Evans S et al (1992) Proton MR spectroscopy of experimental radiation-induced white matter injury. J Comput Assist Tomogr 16:543–548

Zaharchuk G (2012) Arterial spin labeling for acute stroke: practical considerations. Trans Stroke Res 3:228–235